

1 Development, intercomparison and evaluation of an improved 2 mechanism for the oxidation of dimethyl sulfide in the UKCA model

3 Ben A. Cala^{1,*}, Scott Archer-Nicholls^{1,#}, James Weber^{1,§}, N. Luke Abraham^{1,2}, Paul T. Griffiths^{1,2}, Lorrie
4 Jacob¹, Y. Matthew Shin¹, Laura E. Revell³, Matthew Woodhouse⁴, Alexander T. Archibald^{1,2}

5 ¹Yusuf Hamied Department of Chemistry, University of Cambridge, Cambridge, CB2 1EW, UK

6 ²National Centre for Atmospheric Science, Cambridge, CB2 1EW, UK.

7 ³School of Physical and Chemical Sciences, University of Canterbury, Christchurch, New Zealand.

8 ⁴CSIRO Oceans and Atmosphere, Aspendale, 3195, Australia.

9 *Now at Department of Ocean Systems (OCS), NIOZ Royal Netherlands Institute for Sea Research, Texel, the Netherlands

10 #Now at IT Services, University of Manchester, Manchester, M13 9PL, UK.

11 §Now at School of Biosciences, University of Sheffield, S10 2TN, UK.

12
13 Correspondence to: Alexander T. Archibald ata27@cam.ac.uk and Ben. A. Cala ben.cala@nioz.nl
14

15 **Abstract.** Dimethyl sulfide (DMS) is an important trace gas emitted from the ocean. The oxidation of DMS has long been
16 recognised as being important for global climate through the role DMS plays in setting the sulfate aerosol background in the
17 troposphere. However, the mechanisms in which DMS is oxidised are very complex and have proved elusive to accurately
18 determine in spite of decades of research. As a result the representation of DMS oxidation in global chemistry-climate models
19 is often greatly simplified.

20
21 Recent field observations, laboratory and *ab initio* studies have prompted renewed efforts in understanding the DMS oxidation
22 mechanism, with implications for constraining the uncertainty in the oxidation mechanism of DMS as incorporated in global
23 chemistry-climate models. Here we build on recent evidence and develop a new DMS mechanism for inclusion in the UK
24 Chemistry [Aerosol](#) (UKCA) chemistry-climate model. We compare our new mechanism (CS2-HPMTF) to a number of
25 existing mechanisms used in UKCA (including the highly simplified 3 reactions, 2 species, mechanism used in CMIP6 studies
26 with the model) and to a range of recently developed mechanisms reported in the literature through a series of global and box
27 model experiments. Global model runs with the new mechanism enable us to simulate the global distribution of hydroperoxyl
28 methyl thioformate (HPMTF), which we calculate to have a burden of 2.6-26 Gg S (in good agreement with the literature
29 range of 0.7-18 Gg S). We show that the sinks of HPMTF dominate uncertainty in the budget, not the rate of the isomerisation
30 reaction forming it, and that based on the observed DMS/HPMTF ratio from the global surveys during the NAS Atmospheric
31 Tomography mission (ATom), rapid cloud uptake of HPMTF worsens the model-observation comparison. Our box model
32 experiments highlight that there is significant variance in simulated secondary oxidation products from DMS across
33 mechanisms used in the literature, with significant divergence in the sensitivity of the rates of formation of these products to

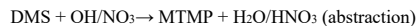
Formatted: Font: Italic

Deleted: Aerosol

35 temperature exhibited; especially for methane sulfonic acid (MSA). Our global model studies show that our updated DMS
36 scheme performs better than the current scheme used in UKCA when compared against a suite of surface and aircraft
37 observations. However, sensitivity studies underscore the need for further laboratory and observational constraints. [In](#)
38 [particular our results suggest that as a priority long-term DMS observations be made to better constrain the highly uncertain](#)
39 [inputs into the system and laboratory studies be performed that address: 1\) the uptake of HPMTF onto aerosol surfaces and](#)
40 [the products of this reaction. 2\) The kinetics and products of the following reactions: CH₃SO₃ decomposition; CH₃S + O₂;](#)
41 [CH₃SOO decomposition; CH₃SO + O₃.](#)
42

43 1 Introduction

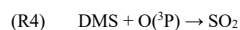
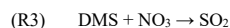
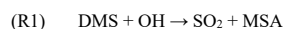
44 It is estimated that 16-28 Tg S year⁻¹ are emitted in the form of dimethyl sulfide (DMS, CH₃SCH₃) from the ocean, making
45 DMS the most abundant biological source of sulfur in the Earth system (Andreae, 1990, Tesdal et al., 2015, Bock et al., 2021).
46 Elucidating the atmospheric fate of DMS has been a long standing goal of the atmospheric chemistry research community
47 owing to a proposed biogeochemical feedback cycle (CLAW; Charlson et al. 1987), whereby DMS oxidation is key to a
48 homeostatic feedback loop. The initial steps in DMS oxidation are well understood (Barnes et al., 2006). Focusing on oxidation
49 via OH (NO₃), the most important oxidant during the daytime (nighttime), DMS is oxidised in the gas-phase through two main
50 pathways: the abstraction pathway forms the methylthiomethylperoxy radical (MTMP, CH₃SCH₂OO) in the first step, while
51 the addition pathway leads to dimethyl sulfoxide (DMSO, CH₃SOCH₃; and to a lesser extent DMSO₂) as an important
52 intermediate.



55 Ultimately, the oxidation of DMS leads to products such as H₂SO₄ and sulfate (SO₄²⁻), as these represent the highest oxidation
56 states of sulfur (S(VI)). Along the way from DMS, a number of secondary oxidation products such as sulfur dioxide (SO₂),
57 methane sulfonic acid (MSA, CH₃SO₃H) and carbonyl sulfide (OCS) can be formed, however the yields of these species
58 depend on the mechanisms involved, which themselves are a function of the chemical (e.g., levels of oxidants) and
59 environmental conditions (e.g., temperature and humidity). The yields of these products are relatively uncertain, with estimates
60 of the DMS-to-SO₂ yield spanning 14-96 % (von Glasow and Crutzen, 2004). The oxidation products can participate in aerosol
61 growth and in new particle formation, affecting the number of cloud condensation nuclei (CCN). As such DMS oxidation can
62 impact cloud formation and lifetime and hence climate; although the absolute effect is still highly uncertain due to the
63 uncertainty in the kinetics and mechanisms of DMS oxidation. Indeed, natural aerosols such as DMS contribute to large
64 uncertainties in the radiative forcing of the pre-industrial atmosphere (Carslaw et al., 2013; Fung et al., 2022).
65

66 Substantial discrepancies between different DMS oxidation mechanisms under different conditions have been found (de Bryn
67 et al., 2002; von Glasow and Crutzen, 2004). The intercomparison study by Karl et al. (2007) looked at seven different
68 chemistry schemes in a box model (using the same inputs) and observed that SO₂ mixing ratios varied from 2 to 44 ppt.
69 Differences between models are even greater when looking at MSA yield (Karl et al., 2007, Hoffmann et al., 2021). The large
70 uncertainties of product ratios indicate the need for more observational constraints for DMS chemistry in models.

71 In the UK Chemistry and Aerosol model (UKCA) two different chemistry schemes are implemented: StratTrop (Archibald et
72 al., 2020), which is a simplified chemistry mechanism included in the UK Earth System Model (Sellar et al., 2019) and CRI-
73 Strat2 (Archer Nicholls et al., 2021; Weber et al., 2021). The DMS oxidation mechanism in StratTrop is, like those used in
74 many Earth System Models (ESMs), a very simple scheme (see S1.4.1 for more details). We believe modellers have opted to
75 keep the DMS chemistry incredibly simple for two main reasons 1) numerical efficiency 2) uncertainty in what to do owing
76 to lack of detailed DMS oxidation mechanisms that have been calibrated against laboratory data. The StratTrop DMS
77 mechanism only includes four reactions and no intermediates for the DMS oxidation scheme.



82 Omitting intermediates might lead to a misrepresentation of the spatial distribution of oxidation products and an overestimation
83 in their formation since the intermediates might be subject to wet and dry deposition or cloud uptake. Because a unity yield of
84 SO₂ is assumed, a change in the distribution of oxidation products due to a changing climate cannot be evaluated.

85

86 CRI-Strat2 (hereafter CS2) (Archer-Nicholls et al., 2021, Weber et al., 2021) is a mechanism that aims to be of intermediate
87 complexity. CS2 includes 19 reactions and 7 intermediates (DMSO, MSIA, MTMP, CH₃S, CH₃SO, CH₃SO₂, CH₃SO₃) as part
88 of its DMS scheme and is primarily based on the work of von Glasow and Crutzen (2004). Whilst the CS2 DMS mechanism
89 is much more complex than the StratTrop scheme, it represents an understanding of DMS chemistry that is far from up-to-
90 date.

91

92 In this work, the gas-phase DMS oxidation by OH and NO₃ in CS2 is updated according to the current scientific understanding.
93 The greatest update is the inclusion of the recently discovered intermediate hydroperoxymethyl thioformate (HPMTF,
94 HOOCH₂SCHO), which is formed through the autoxidation of the methylthiomethyl peroxy radical (MTMP, CH₃SCH₂OO)
95 in the abstraction pathway (Wu et al., 2015, Berndt et al., 2019, Veres et al. 2020). Currently, it is estimated that ~30-50% of
96 DMS yields HPMTF (Veres et al., 2020; Novak et al. (2021); Fung et al. (2022)). There are large uncertainties about the value
97 of $k_{\text{isom},1}$, the rate constant of the first H-shift, which is the rate determining step for HPMTF formation (**Figure 1**). (Note, given
98 that he first isomerization step is rate limiting, the overall rate constant for isomerization is denoted k_{isom}). This determines if

99 autoxidation can compete with or surpass the bimolecular reactions of MTMP with HO₂ and NO. The chamber study by Ye et
00 al. (2021) estimates a probability distribution based on their measurements with one geometric standard deviation spanning an
01 order of magnitude. The isomerization rate constant is predicted using *ab initio* methods to be strongly temperature dependent,
02 indicating that this pathway could be more relevant under a warming climate (Wu et al., 2015; Veres et al., 2020). Following
03 the closure of the Discussion version of this manuscript the first temperature-dependent direct kinetic study of the isomerization
04 of rate constant for MTMP to HPMTF was published (Assaf et al., 2023). In that study the authors calculate the Arrhenius
05 temperature barrier as 7278 ± 99 K, confirming the high temperature dependence of the reaction experimentally.

06
07 As of now, the fate of HPMTF in the atmosphere is largely unknown. Wu et al. (2015) postulate further oxidation with OH,
08 ultimately yielding SO₂ as the dominant product and OCS as a side product. Veres et al. (2020) observe an abrupt decrease of
09 HPMTF mixing ratio in clouds and therefore suggest that heterogeneous loss to aerosol and cloud uptake plays a big role.
10 Vermeuel et al. (2020) support this hypothesis: they find a diurnal profile of HPMTF in the vicinity of California's coast and
11 suggest this is due to the consistent diurnal profile of cloud present. This hypothesis is further supported by the study by Novak
12 et al. (2021), which looks at two case studies and concludes that cloud uptake determines the lifetime of HPMTF. Novak et
13 al. (2021) found that cloud-uptake of HPMTF reduces SO₂ production from DMS by over a third, while providing a more
14 direct pathway to sulfate formation. On the contrary, the chamber study and calculation of Henry's law constant by Wollesen
15 de Jonge et al. (2021) predict that HPMTF does not directly contribute to new particle formation or aerosol growth. Instead,
16 their study proposes aqueous oxidation by OH, ultimately still yielding gas-phase SO₂. Khan et al. (2021) stress the importance
17 of photolysis as a potential loss pathway, which might explain the observed diurnal concentrations throughout the day. Overall,
18 loss processes of HPMTF are poorly understood.

19
20 In this work, we perform a series of updates to the CS₂ DMS oxidation scheme which are evaluated against the current CS₂
21 and the very simplified DMS chemistry in StratTrop. The aim of this work is to improve the representation of DMS chemistry
22 in UKCA and determine the influence of some of the major mechanistic uncertainties on model simulated SO₂ levels compared
23 against ATom observations (Wofsy et al., 2018; Veres et al., 2020). Our study includes a comprehensive set of box model
24 studies, including an intercomparison of our new DMS scheme against other recently reported schemes in the literature, and
25 global 3D simulations with the UKCA model. To complement the work of Fung et al. (2022), sensitivity studies with variable
26 rates of production, and cloud and aerosol uptake of HPMTF are performed to investigate the effects of the uncertainty in
27 HPMTF formation and depletion on the distribution and burden of SO₂ and sulfate (given their importance in climate) using
28 a structurally different model to that they used.

29

30 **2 Methods**

31 **2.1 Model description**

32 **2.1.1 Set up**

33 **Box model**

34 For the box model experiments, BOXMOX (Knote et al., 2015), the box modelling extension to the Kinetic PreProcessor
35 (KPP) (Sandu and Sander, 2006) was used. The initial and background concentrations of the species were set to be
36 representative of the remote marine boundary layer (MBL) (and are detailed in **Table S1**). NO_x concentration was kept at
37 approximately 10 ppt, unless otherwise specified.

38 The box model set up simulates an MBL air parcel exchanging with the free troposphere. The diurnal profile of the planetary
39 boundary layer height was modelled after the diurnal profile of the MBL in Ho et al. (2015) (**Table S2**). Mixing of the air
40 within the box with the free troposphere is described by the increases of box height: it is assumed that changes in the box
41 volume are due to the influx of background air. Emissions of DMS are added at 3.48×10^9 molec. cm⁻² s⁻¹ (consistent with
42 [the higher emission flux in](#) von Glasow and Crutzen (2004)). Emissions mix instantaneously within the box. Temperature
43 varies throughout a 24-hour period between 289-297 K, with a mean of 293 K (**Table S2**). Photolysis reactions are scaled
44 depending on the time of day, and make use of the pre-calculated "J" rates obtained from the MCMv3.3.1. The simulations
45 were run for 192 hours (8 days) with 10-minute time steps. CRI v2.2 R5 (CS2) (Jenkin et al., 2019; Weber et al., 2021) was
46 employed as the base chemical mechanism. Unless otherwise specified, only reactions of the DMS scheme were changed.
47 Neither dry nor wet deposition was included in the box model experiments. The analysis of the BOXMOX simulations
48 discussed in Section 3.1.1 and 3.2.1 focuses on the continuous (hourly) output. In Section 3.1.2 and 3.2.2, simulations with a
49 prescribed temperature (260 - 310 K, step size: 5 K) were conducted. The data from day 7 and 8 of the runs was averaged to
50 enable the effects of changes in the temperature on species concentration simulated in the box model to be calculated (following
51 Archibald et al., 2010)

52

53 **3D simulations**

54 For the 3D simulations we use UKCA, the chemistry and aerosol component of UKESM1, with a horizontal resolution of
55 $1.25^\circ \times 1.875^\circ$ with 85 vertical levels up to 85 km (Walters et al., 2019). UKCA uses the GLOMAP-mode aerosol scheme,
56 which simulates sulfate, sea salt, black carbon (BC), organic matter, and dust but does not currently simulate nitrate aerosol
57 (Mulcahy et al., 2020). Simulations were run for 18 months, using the first 6 months as spin up. In order to look at high time
58 resolution output simulations were re-run for limited time periods using the re-start files of the longer runs but outputting data
59 at hourly frequency.

60

61 Temperature and horizontal wind fields were nudged (Telford et al., 2013) in all model runs to the Era-Interim atmospheric
62 reanalysis from ECMWF (Dee et al., 2011). See the SI for further details.

Deleted: ,

Deleted:).

65

66 The emissions used in this study for UKCA are the same as those from Archer-Nicholls et al (2021) and are those developed
 67 for the Coupled-Model Intercomparison Project 6 (CMIP6) (Collins et al., 2017). See the SI for further details. Oceanic
 68 emissions of DMS are calculated from seawater DMS concentrations (Sellar et al., 2019). In the atmosphere-only setup
 69 employed here seawater DMS concentrations for 2014 from a UKESM1 fully-coupled SSP3-70 ensemble member were
 70 prescribed. The DMS emission flux from the ocean used in the model was 16 Tg S yr^{-1} and therefore on the low end of estimates
 71 of oceanic DMS emissions (e.g., Lana et al., 2011; Bock et al., 2021).

72

73

74 2.1.2 Model runs

75

76 **Table 1:** Configuration of model runs in this study. The last two columns indicate whether this scheme was used for the
 77 BOXMOX experiments or the UKCA runs or both. Additional BOXMOX simulations were performed and the results of which
 78 are included in the Supplementary Information (SI) for completeness.

Alias	Description	Used for:	
		BOXMOX	UKCA
CS2	Base simulation, standard CRIStrat2 (or CRIV2.2R5) scheme	✓	✓
ST	StratTrop chemistry scheme ($ST - CS2 = \Delta ST$; change between ST and CS2)	✓	✓
ST-CS2	StratTrop DMS scheme but CS2 oxidants ($ST - CS2 - CS2 = \Delta CC$; change between CS2 and the ST DMS scheme only)	✓	-
CS2-HPMTF	CS2 + updates in Table 2 and Table 3 ($CS2 - HPMTF - CS2 = \Delta UPD$; effects of all updates made to the scheme)	✓	✓
CS2-UPD-DMS	CS2 + updates in Table 2 = CS2-HPMTF - updates in Table 3 ($CS2 - HPMTF - CS2 - UPD - DMS = \Delta HPMTF$; effects of the isom. pathway only)	✓	-
CS2-HPMTF-CLD	CS2-HPMTF + cloud and aerosol uptake ($\gamma = 0.01$) ($CS2 - HPMTF - CLD - CS2 - HPMTF = \Delta CLD$; gives the effects of cloud and aerosol uptake of HPMTF)	-	✓
CS2-HPMTF-FL	CS2-HPMTF + faster total loss of HPMTF to OH ($5.5 \times 10^{-11} \text{ s}^{-1}$) ($CS2 - HPMTF - FL - CS2 - HPMTF = \Delta FL$; gives the effects of faster gas phase loss of HPMTF)	SI	✓
CS2-HPMTF-FP	CS2-HPMTF + isomerisation A-factor scaled by a factor of 5, see Wollesen de Jonge et al. (2021)) ($CS2 - HPMTF - FP - CS2 - HPMTF = \Delta FP$; gives the effects of faster HPMTF production)	SI	✓

Formatted Table

79

80 Simulations are performed with the standard or updated DMS scheme to quantify the impacts of the mechanistic changes.
81 Details are given in **Table 1**. We chose as our base run a simulation with the CRIStrat2 chemistry scheme hereafter referred
82 to as CS2 (Weber et al., 2021). We perform two simulations with StratTrop (hereafter ST): ST is the default mechanism as
83 used in UKESM1, while ST-CS2 uses the ST DMS chemistry (R1-R4) but all other reactions (HO_x, NO_x, VOC etc) are
84 identical to CS2. This allows us to attribute the changes arising solely to differences in the oxidising capacity/environment
85 (driven by the chemistry not strongly coupled to DMS) and isolate the role due to differences in the DMS reactions themselves.
86
87 In updating the representation of DMS chemistry for UKCA a number of changes were considered. Broadly these fall into two
88 categories: 1) Incorporation of the chemistry of HPMTF (shown in red in **Figure 1**) 2) updates to other aspects of DMS
89 oxidation chemistry (shown in blue in **Figure 1**). CS2-HPMTF is used to identify the fully updated DMS mechanism (**Table**
90 **2, Table 3**). All other runs act as sensitivity runs. CS2-UPD-DMS allows the evaluation of only updating the standard DMS
91 chemistry (**Table 2**), without the addition of the isomerization branch and HPMTF formation (**Table 3**). CS2-HPMTF-CLD
92 adds cloud and aerosol uptake of HPMTF with subsequent sulfate formation, similar to Novak et al. (2021). With CS2-
93 HPMTF-FP and CS2-HPMTF-FL the effects of faster production and faster loss of HPMTF can be assessed.
94
95

2.2 New mechanism development

The current CS2 DMS oxidation mechanism is based on von Glasow and Crutzen (2004). This mechanism is based on an outdated understanding of DMS oxidation, which excludes key pathways and intermediates that are now known to be well established (Barnes et al., 2006) as well as more recent pathways and products that have been shown to be important (Veres et al., 2020). Our aim with the development of the new mechanism is to build upon the existing mechanism in CS2 and to update and extend it. To this end we performed a literature review and constructed a number of mechanistic variants that were examined in a series of box model experiments (see the SI for further details). As with all mechanism development exercises, a series of target compounds were chosen to reduce the mechanism to achieve a scheme that is parsimonious; for use in a 3D chemistry-climate model. In our study we chose DMS, SO₂, sulfate (H₂SO₄) and HPMTF as the key target molecules for mechanism optimization. **Figure 1** shows the two-step improvement of this mechanism. First, the improvement of the standard chemistry by updating rate constants for existing reactions in the scheme or the addition of reactions that were missing (denoted with blue colouring in **Figure 1**), and second, the addition of the HPMTF pathway (in red in **Figure 1**). The focus in this study is on gas-phase DMS oxidation by OH and NO₃. Our prime focus is on the primary oxidation products (DMSO and MTMP) and their subsequent chemistry. While other studies include DMS oxidation by BrO and Cl, the contribution is either negligible or there is a large uncertainty attached due to substantial discrepancies between/within models and measurements of halogens and halogen oxides (Wang et al., 2021; Fung et al., 2022). Moreover, UKCA doesn't currently have a comprehensive tropospheric halogen mechanism and levels of BrO and Cl simulated are much lower than observations suggest.

The updates made to the standard CRIStrat 2 DMS scheme are presented in Tables 2 and 3. Please see the SI S1.2 for a complete description of how these updates were made.

Table 2: Summary of the H-abstraction and OH-addition branches in the DMS oxidation pathway. Reactions in bold are newly added in this work.

No.	Reactions	Rate (cm ³ molecule ⁻¹ s ⁻¹)	Reference
1a	DMS + OH → MTMP + H ₂ O	1.12×10 ⁻¹¹ exp ^(-250/T)	IUPAC SOx22 (upd. 2006)
1b	DMS + NO ₃ → MTMP + HNO ₃	1.90×10 ⁻¹³ exp ^(520/T)	Atkinson et al. (2004)
1c	DMS + OH → DMSO + HO ₂	see note ^a	IUPAC SOx22 (upd. 2006)
2a	MTMP + NO → HCHO + CH ₃ S + NO ₂	4.90×10 ⁻¹² exp ^(263/T)	von Glasow and Crutzen (2004)
2b	MTMP + MTMP → 2 HCHO + 2 CH ₃ S	1.0×10 ⁻¹¹	von Glasow and Crutzen (2004)
2c	MTMP + HO₂ → CH₂SCH₂OOH	2.91×10⁻¹³ exp^(1300/T) × 0.387	MCMv3.3.1
3	CH₂SCH₂OOH + OH → CH₃SCHO	7.03×10⁻¹¹	MCMv3.3.1
4	CH₃SCHO + OH → CH₃S + CO	1.11×10⁻¹¹	MCMv3.3.1
5a	CH ₃ S + O ₃ → CH ₃ SO	1.15×10 ⁻¹² exp ^(432/T)	Atkinson et al. (2004)
5b	CH ₃ S + NO ₂ → CH ₃ SO + NO	3.00×10 ⁻¹² exp ^(210/T)	Atkinson et al. (2004)

Deleted: .

Deleted: 2.2.1 Updating

Deleted: DMS chemistry in

Deleted: ¶

The H-abstraction pathway (reaction 1a,b) generates MTMP which is then further oxidised to SO₂ or CH₃SO₂ (reactions 2-7). The OH-addition pathway (reaction 1c) leads to dimethyl sulfoxide (DMSO, (CH₃)₂SO)

Deleted: methanesulfonic acid (MSIA, CH₃S(O)OH) (reactions 8,9) and further oxidation through to CH₃SO₂ (reactions 10-12). Both pathways and

Deleted: changes made are summarised in **Table 2**. The newly added reactions and their respective rate constants are largely based on Atkinson et al. (2004), the MCMv3.3.1 (Jenkin et al. 2015), and the primary literature therein. ¶

¶ The oxidation of MTMP by HO₂ (reaction 2c) was not previously included in the CS2 mechanism, but is expected to play a significant role at the low NO_x conditions over the remote ocean. Based on other RO₂ + HO₂ reactions, CH₂SCH₂OOH is the expected product, which has been detected through mass spectroscopy (Butkovskaya and LeBras, 1994). Since no experimental measurements exist

Formatted: Right: 0 cm, Line spacing: 1.5 lines

Deleted: the kinetics of this reaction, the rate constant provided in the MCM was used. It is based on a generic expression, defined on the basis of available room temperature and temperature dependent data for alkyl and β-hydroxy RO₂ and it is dependent on the number of carbon atoms. Further oxidation of CH₂SCH₂OOH leads to the formation of methylthiolformate (MTF, CH₃SCHO) (reaction 3), a species that has been detected in chamber studies before under low NO_x conditions (Arsene et al., 1999; Urbanski et al., 1998). MTF decomposes to CH₃S (reaction 4), an intermediate that is already part of the CS2 DMS scheme as a reaction product of MTMP (reaction 2a,b). ¶

Deleted: CH₃S can add an O₂ to form a weakly bound adduct, CH₃SOO (reaction 5c). At 298 K at sea level, approximately one-third of CH₃S is present as the CH₃SOO adduct and at colder temperatures this ratio is even greater (75% at 273 K) (Tumip (... [1])

Deleted: updated accordingly (reaction 7c). Additionally, the branching ratios of CH₃SO oxidation by NO₂ to CH₃SO₂ and SO₂ were revised to also match the findings by Borissenko et al. (2003).

Deleted: ¶

While some CH₃SO₂ stems from the NO₃ oxidation of CH₃SO, it is mainly formed through oxidation of MSIA (reaction 9a,c), (... [2])

Deleted: -1

Deleted: (Campolongo et al., 1999; Sander 2021). We note that Wollesen de Jonge et al. (2021) calculated the Henry's law coefficient to be approximately an order of magnitude lower a (... [3])

Deleted: -1

Deleted: (Barnes et al., 2006). Dry deposition is omitted for DMSO and MSIA since they are expected to be relatively short-lived. ¶

Formatted Table

5c	$\text{CH}_3\text{S} + \text{O}_2 \rightarrow \text{CH}_3\text{SOO}$	$1.20 \times 10^{-16} \exp^{(1580/T)} \times [\text{O}_2]$	Atkinson et al. (2004)
6a	$\text{CH}_3\text{SOO} \rightarrow \text{CH}_3\text{O}_2 + \text{SO}_2$	$5.60 \times 10^{-16} \exp^{(-10870/T)}$	Atkinson et al. (2004)
6b	$\text{CH}_3\text{SOO} \rightarrow \text{CH}_3\text{S} + \text{O}_2$	$3.50 \times 10^{-10} \exp^{(-3560/T)}$	MCMv3.3.1 (based on: McKee (1993), and Butkovskaya and Barnes (2002))
7a	$\text{CH}_3\text{SO} + \text{NO}_2 \rightarrow \text{CH}_3\text{SO}_2 + \text{NO}$	$1.2 \times 10^{-11} \times 0.75$	Borrisenko et al. (2003), Atkinson et al. (2004)
7b	$\text{CH}_3\text{SO} + \text{NO}_2 \rightarrow \text{SO}_2 + \text{CH}_3\text{O}_2 + \text{NO}$	$1.2 \times 10^{-11} \times 0.25$	Borrisenko et al. (2003), Atkinson et al. (2004)
7c_old	$\text{CH}_3\text{SO} + \text{O}_3 \rightarrow \text{CH}_3\text{SO}_2$	6.0×10^{-13}	Von Glasow and Crutzen (2004)
7c	$\text{CH}_3\text{SO} + \text{O}_3 \rightarrow \text{CH}_3\text{O}_2 + \text{SO}_2$	4×10^{-13}	Borrisenko et al. (2003), IUPAC SOx61 (upd. 2006)
8	$\text{DMSO} + \text{OH} \rightarrow \text{MSIA} + \text{CH}_3\text{O}_2$	$8.7 \times 10^{-11} \times 0.95$	von Glasow and Crutzen (2004)
9a	$\text{MSIA} + \text{OH} \rightarrow \text{CH}_3\text{SO}_2 + \text{H}_2\text{O}$	$9.0 \times 10^{-11} \times 0.95$	von Glasow and Crutzen (2004)
9b	$\text{MSIA} + \text{OH} \rightarrow \text{MSA} + \text{HO}_2 + \text{H}_2\text{O}$	$9.0 \times 10^{-11} \times 0.05$	von Glasow and Crutzen (2004)
9c	$\text{MSIA} + \text{NO}_3 \rightarrow \text{CH}_3\text{SO}_2 + \text{HNO}_3$	1.0×10^{-13}	von Glasow and Crutzen (2004)
10a	$\text{CH}_3\text{SO}_2 \rightarrow \text{CH}_3\text{O}_2 + \text{SO}_2$	$5.0 \times 10^{-13} \exp^{(-9673/T)}$	MCMv3.3.1 (based on: Barone et al. (1995))
10b	$\text{CH}_3\text{SO}_2 + \text{O}_3 \rightarrow \text{CH}_3\text{SO}_3$	3.0×10^{-13}	von Glasow and Crutzen (2004)
10c	$\text{CH}_3\text{SO}_2 + \text{NO}_2 \rightarrow \text{CH}_3\text{SO}_3 + \text{NO}$	2.2×10^{-12}	Atkinson et al. (2004)
11a	$\text{CH}_3\text{SO}_3 + \text{HO}_2 \rightarrow \text{MSA}$	5.0×10^{-11}	von Glasow and Crutzen (2004)
11b_old	$\text{CH}_3\text{SO}_3 \rightarrow \text{CH}_3\text{O}_2 + \text{H}_2\text{SO}_4$	$1.36 \times 10^{14} \exp^{(-11071/T)}$	von Glasow and Crutzen (2004)
11b	$\text{CH}_3\text{SO}_3 \rightarrow \text{CH}_3\text{O}_2 + \text{SO}_3$	$5.0 \times 10^{13} \exp^{(-9946/T)}$	MCMv3.3.1 (based on: Barone et al. (1995))
12	$\text{MSA} + \text{OH} \rightarrow \text{CH}_3\text{SO}_3$	2.24×10^{-14}	MCMv3.3.1

$$^a 9.5 \times 10^{-39} \exp^{(5270/T)} [\text{O}_2] / (1 + 7.5 \times 10^{-29} \exp^{(5610/T)} [\text{O}_2])$$

Table 3: Summary of the isomerization branch of the H-abstraction pathway. Rate constants referenced to this work are described in Section [S1.2.1 of the SI](#).

No.	Reaction	Rate ($\text{cm}^3 \text{ molecule}^{-1} \text{ s}^{-1}$)	Reference
2d	$\text{MTMP} \rightarrow \text{HPMTF} + \text{OH}$	see note ^a	Veres et al. (2020)
13a	$\text{HPMTF} + \text{OH} \rightarrow \text{HOCH}_2\text{S} + \text{H}_2\text{O} + \text{CO}$	$1.0 \times 10^{-11} \times 0.9$	this work
13b	$\text{HPMTF} + \text{OH} \rightarrow \text{OCS} + \text{OH} + \text{HCHO} + \text{H}_2\text{O}$	$1.0 \times 10^{-11} \times 0.1$	this work
14a	$\text{HOCH}_2\text{S} + \text{O}_3 \rightarrow \text{HOCH}_2\text{SO}$	$1.15 \times 10^{-12} \exp^{(430/T)}$	Wu et al. (2015)
14b	$\text{HOCH}_2\text{S} + \text{NO}_2 \rightarrow \text{HOCH}_2\text{SO} + \text{NO}$	$6.00 \times 10^{-11} \exp^{(240/T)}$	Wu et al. (2015)
14c	$\text{HOCH}_2\text{S} + \text{O}_2 \rightarrow \text{HOCH}_2\text{SOO}$	$1.20 \times 10^{-16} \exp^{(1580/T)} \times [\text{O}_2]$	this work
15a	$\text{HOCH}_2\text{SOO} \rightarrow \text{HOCH}_2\text{S} + \text{O}_2$	$3.50 \times 10^{-10} \exp^{(-3560/T)}$	this work
15b	$\text{HOCH}_2\text{SOO} \rightarrow \text{HCHO} + \text{OH} + \text{SO}_2$	$5.60 \times 10^{-16} \exp^{(-10870/T)}$	this work
16a	$\text{HOCH}_2\text{SO} + \text{O}_3 \rightarrow \text{HCHO} + \text{OH} + \text{SO}_2$	4×10^{-13}	Wu et al. (2015)
16b	$\text{HOCH}_2\text{SO} + \text{NO}_2 \rightarrow \text{HCHO} + \text{OH} + \text{NO} + \text{SO}_2$	1.2×10^{-11}	Wu et al. (2015)

Deleted: ¶

2.2.2 The addition of the isomerization branch ¶

Following the discovery of HPMTF (Veres et al., 2020) the pathway forming this molecule has now been well established (Wu et al., 2015; Veres et al., 2020; Berndt et al., 2019; Ye et al., 2021). The reactions of the isomerization branch that were added to CS2 (summarised in **Figure 1** and **Table 3**) were identified as those most important in determining SO_2 and HPMTF concentrations through sensitivity studies conducted using our box model setup.

Deleted: Details of these box model sensitivity studies (and the discarded reaction pathways that were found to not be significant) are included in the supplement.

Deleted: In this sense, species like $\text{HOCH}_2\text{SCH}_2\text{OOH}$

Deleted: , included in the studies by Khan et al. (2021)

Deleted: were neglected from our mechanism as this was found to have minor impact on the SO_2 and HPMTF simulated in the box model experiments. The reactions that were added include the autooxidation of MTMP to HPMTF in one step (reaction 2d) and the oxidation of HPMTF by OH, forming OCS (reaction 13b) and HOCH_2S (reaction 13a) with further oxidation to SO_2 (reactions 14-16). The equilibrium with the O_2 -adduct, HOCH_2SOO , and its subsequent decomposition (reaction 14c, 15a,b) was included with kinetics equivalent to CH_3SOO (reaction 5c, 6a,b). Photolysis was found to be a minor pathway of HPMTF loss in our marine boundary layer box model setup (< 10%) and was omitted from the final mechanism used here; contrary to the importance of photolysis of HPMTF found by Khan et al. (2021). ¶

Dry deposition of HPMTF is set using the same parameters in UKCA as other soluble gas-phase compounds, such as CH_3OOH and H_2O_2 , which yield an average deposition velocity similar to the observations of Vermeuel et al. (2020) of 0.75 cms

Deleted: -1

Deleted: For wet deposition of HPMTF, the Henry's law coefficient calculated by Wollesen de Jonge et al. (2021) was used. ¶

For the sensitivity runs described in **Table 1**, some changes are made to the values in **Table 3**. In DMS-HPMTF-FP, the rate constant of reaction 2d is scaled by a factor of 5.0; Berndt et al. (2019) experimentally determined the rate constant at 295 K as 0.23 s^{-1} . Here the A-factor is scaled to match this value, while keeping the temperature dependence calculated by Veres et al. (2020) (following Wollesen de Jonge et al. (2021)). DMS-HPMTF-FL uses a rate constant 5.5 times faster for the total loss of HPMTF to OH (reaction 13a,b), which was recommended as an upper bound by Vermeuel et al. (2020) and following Khan et al. (2021). This range, between the base rate constant and the faster loss, puts us in the middle of the value experimentally determined by Ye et al. (2022). In the remaining sensitivity run CS2-HPMTF-CLD, heterogeneous uptake to both clouds and aerosols was added with reactive uptake coefficient (γ) of 0.01 (following Novak et al., 2021). ¶

Deleted: 2

Formatted Table

.87 $a 2.24 \times 10^{+11} \exp(-9800/T) \exp(1.03e8/(T \times T \times T))$

.88

.89 **2.3 Description of observational data**

.90 **2.3.1 The NASA Atmospheric Tomography (ATom) mission**

.91 An observational dataset used to compare with the model simulations stems from the fourth flight campaign of the NASA
.92 Atmospheric Tomography mission (ATom-4). ATom-4 took place during April and May 2018, and completed a global circuit
.93 around the Americas: from the Arctic to the Antarctic over the remote Pacific and Atlantic Ocean at varying altitudes up to 12
.94 km. A vast number of atmospheric species were measured, including DMS, HPMTF, and SO₂ (Wofsy et al., 2018).

.95

.96 In order to compare the 3D model outputs with the data from the ATom-4 campaign, the hourly outputs from the respective
.97 model runs were interpolated in regards to time and space to generate the data along the flight path. Only model data at times
.98 where valid atmospheric measurements were available are taken into account, resulting in 313 data points for DMS (Whole
.99 Air Sampling) and 36,652 for SO₂ (Laser Induced Fluorescence).

.00

.01 **2.3.2 Surface observations**

.02 Other observational measurements are monthly averages (mean) from the years 1990 to 1999 for DMS measurements made
.03 on Amsterdam Island (37°S, 77°E) in the southern Indian Ocean (Sciare et al., 2000) and the monthly means from 1991 to
.04 1995 for sulfate at the Dumont d'Urville station (66°S, 140°E) at the coast of Antarctica (Minikin et al., 1998). The diel profile
.05 of HPMTF as measured at Scripps Pier in July 2018 was taken from Vermeuel et al. (2020). See the SI for the analysis of the
.06 modelled and observed DMS mixing ratios.

.07 **3 Comparison of DMS oxidation pathways (BOXMOX)**

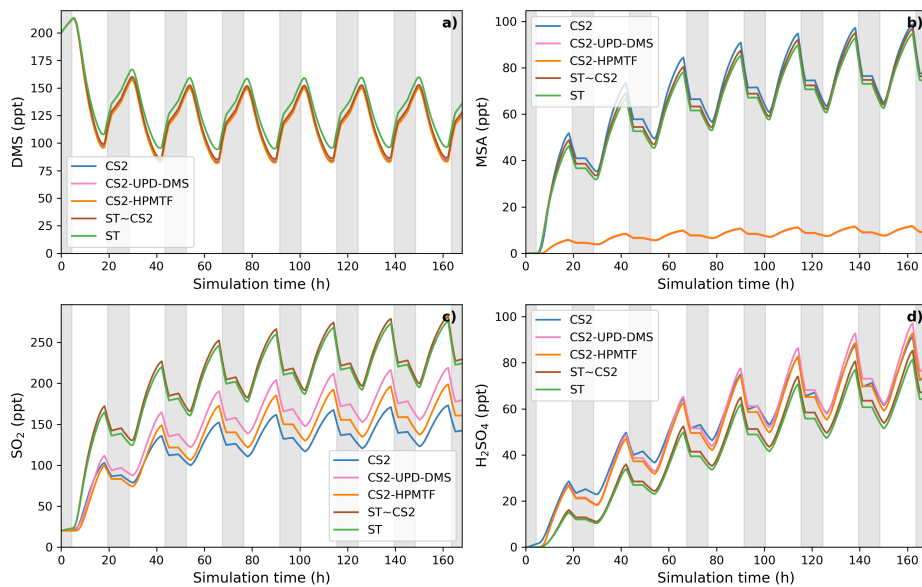
.08 Here we present the results of a series of box model simulations using the BOXMOX model (Weber et al., 2020). With
.09 BOXMOX we look at the diversity in results from simulations using a range of mechanisms, including our newly developed
.10 mechanism. These simulations are not constrained to observations or simulation chamber data. The set-up of the BOXMOX
.11 simulations is described in Section 2.1.1. We focus the analysis here on DMS and its major oxidation products and the effects
.12 of temperature and [NO_x] on these. Section 3.1 compares DMS mechanisms based around the CS2 and ST schemes used in
.13 UKCA (**Table 1**). In Section 3.2 our newly developed mechanism is compared to other DMS mechanisms from recent literature
.14 that also include HPMTF formation.

15 3.1 Comparison of DMS mechanisms used for UKCA

16 3.1.1 Time series analysis

17 The BOXMOX set up allows a quasi steady-state to be achieved for a number of key sulfur species with the main exception
18 being H₂SO₄, which builds up over time in the model as the model is run without aerosol formation and aerosol microphysics
19 included (**Figure 2**). The DMS concentration simulated with different DMS mechanisms used in UKCA is simulated to be
20 very similar throughout all model runs; the small variations stem from different oxidant concentrations or small differences in
21 the rate constants used for the initiation reaction in the different mechanisms (**Figure 2a**). For instance, the ST run has higher
22 DMS concentration because the NO_x concentration is lower (as is OH) and less DMS is oxidised.

23 The SO₂ concentration is increased and MSA is significantly decreased in the updated CS2 runs (CS2-HPMTF and CS2-UPD-
24 DMS) compared to CS2 (**Figure 2b,c**). Comparing CS2-HPMTF and CS2-UPD-DMS, we can see that this pattern (increased
25 SO₂ and decreased MSA) is due to reaction 7c, which directly forms SO₂ and suppresses CH₃SO₂, consequently lowering
26 MSA formation. The SO₂ concentration is lower in CS2-HPMTF compared to CS2-UPD-DMS because the addition of
27 HPMTF produces OCS which acts as a long-lived sulfur reservoir. While MSA concentration is very similar between CS2 and
28 ST, SO₂ concentration is not. This is primarily explained through the difference in the treatment of MSA and SO₂ production
29 in CS2 and ST. MSA is not treated as a reactive species in CS2 and ST (in so much as there are no further reactions of MSA
30 after its production). In ST and ST-CS2, 100% of DMS yields SO₂, regardless of the amount of MSA production. However,
31 as more MSA is produced in CS2 the SO₂ yield is lowered. In spite of higher SO₂ concentrations in the ST DMS schemes, this
32 trend does not translate to H₂SO₄ concentration (**Figure 2d**). SO₂ is a relatively long-lived species (~2 days in our model but
33 with a range from 0.5-2.5 days (Lee et al., (2011))) and can therefore be lost through the mixing processes with the background
34 air in the BOXMOX setup. In CS2, CH₃SO₃ decomposition provides a direct pathway to H₂SO₄ production. In the updated
35 CS2 schemes (CS2-UPD-DMS and CS2-HPMTF) SO₃ production with instantaneous transformation to H₂SO₄ is included.
36 The slower rate constant in CS2 for the decomposition of CH₃SO₃ (11b_old) is compensated by a higher production of CH₃SO₃.



.37

.38 **Figure 2:** BOXMOX-simulated gas-phase concentrations as a function of time for a selection of species simulated with the
 .39 different DMS gas-phase oxidation schemes used in UKCA configurations (oxidation by OH and NO₃). Grey areas denote
 .40 nighttime, when no photolysis reactions are taking place. Average NO_x concentration is approximately 10 ppt, with an average
 .41 temperature of 293 K (range: 289 – 297 K).
 .42

.43

3.1.2 Sensitivity of UKCA DMS schemes to temperature

.44 As described in Section 2.1.1, a series of BOXMOX experiments were performed perturbing the temperature profile in the
 .45 model (**Figure 3**).
 .46

.47 As temperature increases in the box model, the steady-state DMS concentration increases in all simulations. This is mainly
 .48 because the DMS oxidation by OH addition is negatively temperature dependent. For most models, DMS concentration
 .49 increases by 85-93 ppt throughout the temperature range from 260 K to 310 K, except the ST run where at temperatures over
 .50 290 K, a stronger increase of DMS concentration is found, with a total increase of 106 ppt. This could be due to different

.51 oxidant concentrations in the model runs using the ST mechanism and independent of the DMS scheme since this stronger
.52 increase is not found with CS2-ST.

.53 Although the kinetics, and therefore temperature dependence, of DMS loss is comparable across the different schemes, the
.54 dependence of MSA and SO₂ on temperature differ significantly.

.55

.56 Most MSA is formed from the OH-addition channel, which is favoured at low temperatures (Barnes et al., 2006). Therefore,
.57 the MSA concentration is higher at lower temperatures across all the UKCA DMS schemes considered (**Figure 3b**). In the ST
.58 schemes (ST and ST~CS2), MSA decreases by around 88% (-189 ppt and -197 ppt) throughout the temperature range
.59 considered, while in all the CS2 schemes MSA is shown to be much more sensitive to temperature, decreasing by >96% (CS2:
.60 -300 ppt, CS2-UPD-DMS: -222 ppt, CS2-HPMTF: -222 ppt) between 270 to 290 K. We attribute this to differences in the
.61 rate constant of DMS oxidation through the OH-addition channel (see **Table 2** and **S1.4.1**) used in the UKCA ST schemes and
.62 the UKCA CS2 schemes. The expression used in the ST family of schemes (the provenance of which is Pham et al. (1995),
.63 see S1.4.1) has a much shallower gradient with temperature than the expression used in the CS2 family of schemes (which is
.64 based on the latest IUPAC recommendation). The average MSA concentration for the UKCA schemes diverges most in the
.65 temperature range between 270 - 300 K.

.66

.67 The difference in SO₂ concentrations between the CS2 schemes and ST schemes are greatest at lower temperature (**Figure**
.68 **3c**), with the ST and CS2-ST schemes simulating ~ 5 times (+200 ppt) the SO₂ that is simulated in the other schemes based
.69 around CS2. In the ST schemes SO₂ concentration either stays at a similar level across the whole temperature range (ST: +3%)
.70 or slightly decreases (ST~CS2: -9%). Conversely, the CS2 family of schemes show a positive temperature dependence (i.e.,
.71 $+\frac{d[x]}{dT}$), across the temperature range, especially in the range of relevant atmospheric temperatures from 270 to 290 K. SO₂
.72 increases by 298% in CS2, 84% in CS2-UPD-DMS and 79% CS2-HPMTF. In the CS2 schemes, more DMS reacts through
.73 the addition pathway which favours the production of MSA, instead of SO₂ therefore reducing the SO₂ concentration. In ST,
.74 the addition pathway still leads to 100% SO₂ formation, making the average SO₂ concentration less dependent on temperature.
.75 Experimental findings (Arsene et al., 1999) and field measurements (Sciare et al., 2001) both show a positive temperature
.76 dependence of SO₂ concentration. This trend is only reproduced by the DMS schemes based on the CS2 mechanistic features
.77 (i.e. not the very simple mechanism used in ST), indicating that the ST DMS chemistry is likely insufficient to explain
.78 laboratory and field observations, particularly in cold environments and under climate change.

.79

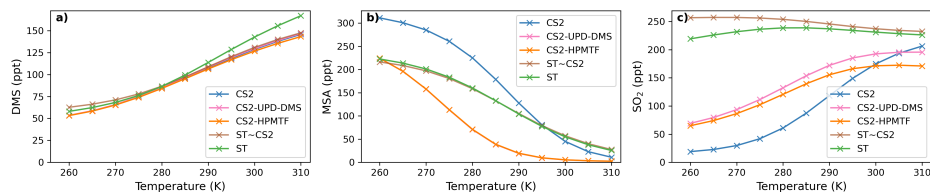
.80 In these box model experiments only gas phase losses and mixing of species with background air are considered. Under the
.81 conditions of our simulations, we find that the MTMP isomerization pathway mainly yields SO₂, as does the rest of the
.82 abstraction pathway. Therefore, the addition of the isomerization branch does not have a significant impact on the temperature

Deleted:). In particular the CS2 family of mechanisms shows pronounced temperature sensitivity

Deleted: 3

Deleted:).

.87 dependence of SO₂ concentration (comparing CS2-UPD-DMS and CS2-HPMTF), even though the isomerization step itself is
.88 greatly temperature dependent.



.89
.90 **Figure 3:** Temperature dependence of average a) DMS, b) MSA, and c) SO₂ concentration after a quasi steady-state is reached
.91 in the box model simulations using the DMS schemes for UKCA.
.92

.93 3.2 Comparison with DMS schemes that include HPMTF from the recent literature

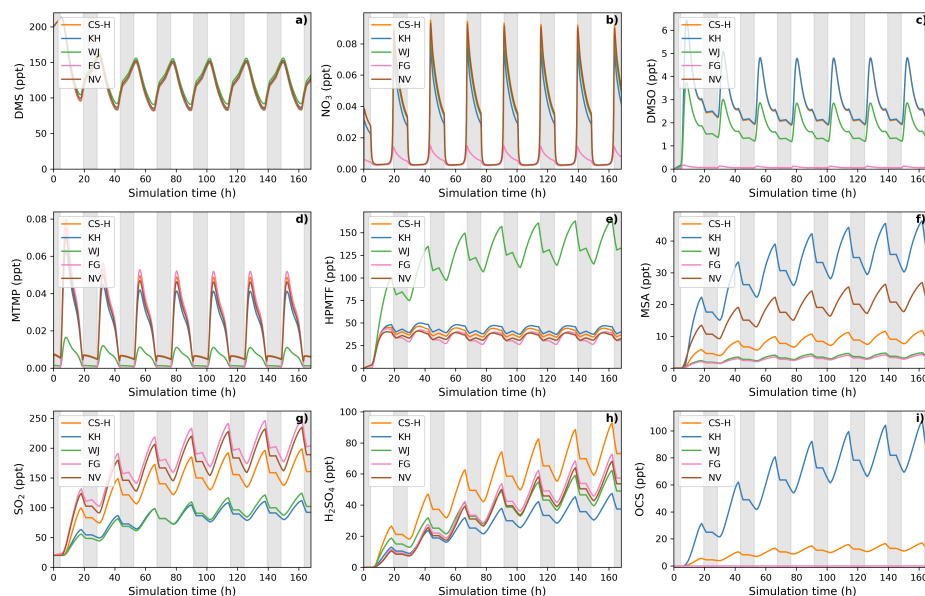
.94 Here, four recently published DMS schemes that also include the isomerization pathway and formation of HPMTF are
.95 compared with our new mechanism, CS2-HPMTF (*CS-H*, 36 reactions in DMS scheme), as follows. To make the studies
.96 comparable, only DMS oxidation by NO₃ and OH and gas-phase reactions are considered. The implementation of these
.97 chemical schemes in BOXMOX can be found in the *Supporting Information S1.3*.

- .98 • *Fung et al. (2022) (FG)*: This scheme includes 32 reactions for the DMS oxidation chemistry. The H-abstraction
.99 pathway is based on the MCM, while the rate constants in the OH-addition pathway mostly stem from Burkholder et
.00 al. (2015) or a scaled up version of those. The rate constant of MTMP isomerization to HPMTF is based on Veres et
.01 al. (2020).
- .02 • *Wollesen de Jonge et al. (2021) (WJ)*: This scheme is the most complex and consists of 98 reactions, including
.03 reactions from the MCM and from Hoffmann et al. (2016). The isomerization branch mostly uses the rate constants
.04 by Wu et al. (2015), except the first isomerization rate constant, which is a combination of Veres et al. (2020) and
.05 Berndt et al. (2019).
- .06 • *Khan et al. (2021) (KH)*: This scheme is based on Khan et al. (2016), which is equivalent to the DMS chemistry in
.07 CS2 (CRI v2 R5). The mechanism was modified to include the isomerization pathway and photolysis loss and
.08 temperature dependent OH oxidation of HPMTF by the authors. In total, the DMS chemistry consists of 38 reactions,
.09 5 of which are photolysis reactions.
- .10 • *Novak et al. (2021) (NV)*: This is a simplified scheme that aims to only include the intermediates necessary for
.11 HPMTF formation and consists of only 10 reactions. DMS therefore either directly yields MSA (without DMSO
.12 formation) or first forms MTMP, which isomerizes to form HPMTF or is oxidised to SO₂.

.13

14 Using this ensemble of gas-phase DMS oxidation schemes in BOXMOX simulations leads to significant differences in the
 15 concentrations of important oxidation intermediates and products, even though DMS concentration is similar across all models
 16 (Figure 4).

17 3.2.1 Time series analysis of different DMS-HPMTF schemes



18 **Figure 4:** Gas-phase concentrations as a function of time for different DMS gas-phase oxidation schemes (oxidation by OH
 19 and NO₃). Average NO_x concentration is approximately 10 ppt, with an average temperature of 293 K (range: 289 – 297 K).
 20 and NO₃). Average NO_x concentration is approximately 10 ppt, with an average temperature of 293 K (range: 289 – 297 K).
 21 Grey areas denote nighttime when no photolysis reactions are taking place.
 22
 23

24 The depletion of DMS due to OH and NO₃ oxidation is similar across most models (Figure 4a) since the major oxidants are
 25 relatively constrained by the box model experiment set up (see Section 2.1.1) and they mostly rely on IUPAC or JPL
 26 recommended values (Atkinson et al., 2004; Burkholder et al., 2015). One exception is NO₃ oxidation in the FG scheme, which
 27 uses a rate constant a factor of approximately 6 higher than the JPL recommendation. On the one hand, this does not affect
 28 DMS concentration, since OH oxidation of DMS plays a greater role, on the other hand, the concentration of NO₃ in the FG

29 scheme's simulation run is controlled by the greater NO_3 oxidation rate (**Figure 4b**). WJ includes the intermediate
30 $\text{CH}_3\text{S}(\text{OH})\text{CH}_3$ and its decomposition back to DMS (based on Hoffmann et al., (2016)), which in their experiments improved
31 the fit between their measured and modelled DMS concentration. Here, this does not have any significant impact on DMS
32 concentration, compared to all the other schemes.

33
34 Significant differences between the models can be found for the DMSO concentration (**Figure 4c**). KH and CS-H have the
35 highest DMSO concentration since all DMS that is oxidised through the OH-addition pathway yields DMSO. This is not the
36 case for WJ, where CH_3SOH and to a small part DMSO_2 are also possible products. In the FG simulation, DMSO concentration
37 is close to zero, which is due to a much faster loss of DMSO; a rate constant a factor of 15 faster than experimental
38 measurements by Urbanski et al. (1998). NV does not include DMSO as an intermediate. Since the lifetime of DMSO was
39 found to be several hours (Urbanski et al., 1998; Ye et al. 2021), deposition of DMSO could act as a significant sink of
40 atmospheric sulfur (as found by Chen et al. (2018)). Fast oxidation of DMSO in FG, or omitting the species in NV, might
41 therefore lead to an over-estimation of other DMS oxidation products in those schemes.

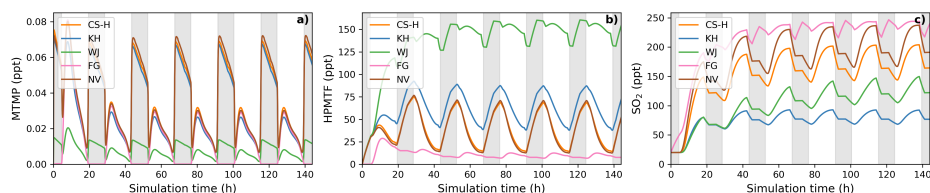
42
43 Regarding the intermediate MTMP, WJ shows the greatest deviation from the ensemble (**Figure 4d**). The MTMP concentration
44 never exceeds 0.02 ppt in WJ, while the other mechanisms simulate concentrations over three times higher. WJ employs a
45 faster isomerization rate constant of MTMP to HPMTF. They scale the A-factor by 5 to get a rate constant that is a combination
46 of the theoretical calculations by Veres et al. (2020) and the experimental findings by Berndt et al. (2019). Additionally, they
47 include more oxidation reactions of MTMP (such as oxidation by NO_3) but since the isomerization to HPMTF already
48 outcompetes most oxidation reactions anyway (>97%), we found them to play a negligible role (<0.1%). In the FG scheme,
49 $\text{DMS} + \text{NO}_3$ leads to immediate SO_2 formation, without prior MTMP formation. Therefore, no MTMP is produced during the
50 nighttime, when NO_3 oxidation becomes relevant. Under conditions with low NO_x (around 10 ppt in this experiment) this does
51 not have significant impacts but at higher NO_x concentrations this leads to a major deviation from the other simulations (**Figure**
52 **5a**, 100 ppt NO_x). At night, CS-H, KH, and NV reach MTMP concentrations of 0.07 ppt, allowing nighttime HPMTF
53 formation, while FG stays zero.

54
55 All model simulations, except WJ, are very similar in HPMTF concentration (**Figure 4e**). The fast isomerization rate constant
56 in WJ is one of the reasons HPMTF concentration is on average more than 3 times higher than the other model simulations.
57 The other reason is a much slower oxidation of HPMTF by OH. While most models use a value of (or close to) 1.11×10^{-11}
58 $\text{cm}^3 \text{ molecule}^{-1} \text{ s}^{-1}$, recommended by Vermeuel et al. (2020), WJ use the much slower rate constant calculated by Wu et al.
59 (2015), $1.4 \times 10^{-12} \text{ cm}^3 \text{ molecule}^{-1} \text{ s}^{-1}$. This rate constant is also used in the KH scheme but it additionally includes HPMTF
60 depletion by photolysis which ultimately leads to the similar HPMTF concentration as in CS-H, FG, and NV. The addition of
61 the photolysis reactions in KH does not affect the diel profile of HPMTF, even though those account for 81% of chemical loss
62 of HPMTF in their scheme. It is therefore unlikely that the observed diel profile of HPMTF by Vermeuel et al. (2020) and

63 Khan et al. (2021) can be explained solely by considering loss of HPMTF to aldehyde and hydroperoxide photolysis. Reducing
64 HPMTF formation to one isomerization reaction without any side reactions as is done in this work and NV, does also not affect
65 the diel profile of HPMTF significantly.

66 The effect of higher NO_x conditions on the diel profile of HPMTF varies significantly between the different schemes (10 ppt
67 NO_x in **Figure 4** vs. 100 ppt NO_x in **Figure 5**). Higher NO_x concentration leads to more DMS oxidation by NO₃ at night and
68 the subsequent increase in MTMP concentration and therefore HPMTF concentration during the night hours in the CS-H, WJ,
69 KH, and NV simulations. At low NO_x, HPMTF concentration stayed more or less stable throughout the nighttime and increased
70 in the morning, reaching a plateau in the afternoon, and dropping in the evening (**Figure 4e**). Under higher Nox conditions,
71 HPMTF increases in these mechanisms throughout the night and decreases throughout the day when it is oxidised by OH
72 (**Figure 5b**). In the WJ simulation, the diel profile has more plateaus and small deviances but the overall trend still fits the
73 described pattern. This is not true for FG, where DMS oxidation by NO₃ leads directly to SO₂ formation.

74



75

76 **Figure 5:** BOXMOX simulations where the average NO_x concentration is approximately 100 ppt (a factor 10 greater than for
77 the results presented in **Figure 4**). (a) MTMP, (b) HPMTF, and (c) SO₂ concentration as a function of time for different DMS
78 gas-phase oxidation schemes (oxidation by OH and NO₃). Average temperature of 293 K (range: 289 – 297 K). Grey areas
79 denote nighttime when no photolysis reactions are taking place.

80

81 While the diel profile of MSA looks similar for all simulations, the average concentrations do not (**Figure 4f**). The highest
82 average steady-state MSA concentration is reached in the KH simulation, which is a factor of 10 higher than the lowest average
83 concentration in the FG simulation. In our experimental setup, most of the simulations we performed with the different
84 mechanisms do not include any (significant) gas-phase chemical loss pathway for MSA; MSA is only lost through mixing and
85 transport out of the “box”. Therefore, the concentration of MSA is a direct reflection of MSA production in the respective
86 simulations.

87

88 KH simulates the highest production of MSA (similar to CS2), where MSA is formed through the addition (MSIA + OH →
89 0.05 MSA + 0.95 CH₃SO₂, reaction 9b,c) and the abstraction channel (CH₃SO + O₃ → CH₃SO₂, reaction 7c_old) of DMS
90 oxidation, with CH₃SO₂ partly being oxidised to CH₃SO₃ and then to MSA (reactions 10b,c, 11a). The decomposition of

i91 CH₃SO₃ to H₂SO₄ in KH is slower than in other mechanisms, increasing the branching ratio for MSA formation in their
i92 mechanism. In NV, the simulation with the second highest average MSA concentration, the only source of MSA is the direct
i93 production of MSA through OH oxidation through the addition channel, where 25% of DMS forms MSA. In both, CS-H and
i94 WJ, the abstraction pathway mostly produces SO₂ and only contributes negligible amounts to CH₃SO₂ formation, hence MSA.
i95 Similar to KH, the oxidation of DMS through the addition pathway in CS-H and WJ yields CH₃SO₂ of which a part forms
i96 MSA. However, not all of the CH₃SO₂ results in MSA, some of it also decomposes to SO₂ or yields SO₃. This explains the
i97 lower concentration of MSA in CS-H and WJ compared with NV. The reason why CS-H has a higher MSA concentration than
i98 WJ is because of the inclusion of reaction 9b (**Table 2**), which yields MSA directly and is not part of the WJ scheme.
i99 The lowest MSA concentration is found in FG and WJ, where 60% of the OH-addition pathway directly produces SO₂. Out of
i00 the 40% of DMS that forms DMSO in this pathway, only a fraction yields MSA.

i01
i02 To harmonise the results and aid interpretability, the same rates (based on CS2) are used for the loss processes of SO₂ in all
i03 the mechanisms considered here, therefore the concentration of SO₂ can be used as a proxy for SO₂ production, just as for
i04 MSA. The highest SO₂ concentration can be seen in schemes that have the smallest number of intermediates or the most direct
i05 pathways from DMS to SO₂, in NV and FG (**Figure 4g**). Fewer intermediates result in less opportunities for the formation of
i06 side products or less long-lived species that can be lost through transport or deposition. For instance, in WJ HPMTF is lost
i07 through mixing with the background before it can form SO₂. Likewise, KH has a higher ratio of MSA and OCS production,
i08 which lowers the SO₂ yield. The diel profile of SO₂ concentration is in most simulations not affected by higher NO_x
i09 concentrations, with the general trend being an increase of SO₂ concentration during the day and a decrease at night (**Figure**
i10 **5c**). The only exception is the FG simulation, where we see a clear increase through part of the night, due to the reaction DMS
i11 + NO₃ → SO₂.

i12
i13 The H₂SO₄ concentration is influenced by SO₂ production and CH₃SO₃ production and the rate of decomposition of SO₃ to
i14 H₂SO₄. CS-H has the highest average H₂SO₄ concentration and KH the lowest; all other models are very similar to each other
i15 (**Figure 4h**). In general, higher SO₂ concentration leads to more H₂SO₄, since SO₂ is first oxidised to SO₃ and then to H₂SO₄
i16 with the same rates across all schemes. However, all models except NV include an additional pathway of H₂SO₄ formation: in
i17 KH and FG, H₂SO₄ is directly formed from CH₃SO₃, while in CS-H and WJ CH₃SO₃ decomposes to SO₃ first, which then
i18 instantly reacts to H₂SO₄. In KH, the rate constant for the decomposition of CH₃SO₃ at 295 K is a factor of 15 slower than in
i19 the other models. Since the SO₂ concentration is also relatively low, it explains why KH has the lowest H₂SO₄ concentration
i20 of all schemes when reaching steady-state. CS-H results in a higher H₂SO₄ concentration than FG or NV even though those
i21 models have a higher SO₂ concentration. The reason is a higher production of CH₃SO₃ that is then decomposed to SO₃ and
i22 H₂SO₄.

i23

Similar to the other products of the DMS scheme, the concentration of OCS is a reflection of its production. OCS is only produced from oxidation of HPMTF by OH and, in the KH scheme, through photolysis of HPMTF. In KH, 60% of HPMTF forms OCS, resulting in the highest OCS concentration (**Figure 4i**). This stems mainly from the large contribution of the photolysis reactions. Potentially, the rate constant of OH oxidation of HPMTF in KH is too low and therefore OCS might be overestimated. In CS-H, 10% of HPMTF is oxidised to OCS, resulting in an OCS concentration that is on average 5.5 times lower than KH. FG and WJ both use the theoretically determined branching ratio by Wu et al. (2020), which results in only 0.007% of HPMTF being oxidised to OCS at 295 K. NV does not include this pathway. Very recent evidence suggests that there is a small (2%) but prompt source of OCS following the formation (and decomposition) of HPMTF as well as a significant OCS yield (13%) from the HPMTF + OH reaction (Jernigan et al., 2022). These new data were not assessed (or included) in this work but we estimate that inclusion of these mechanistic pathways would result in OCS yields higher than CS-H and the other mechanisms (which have used a very small yield in the past) but consistently lower than that simulated by KH. To summarise, the intercomparison of recent gas-phase DMS oxidation mechanisms complements and extends earlier studies on DMS (Karl et al., 2007). Recent gas-phase DMS oxidation schemes used in modelling studies lead to a wide range in results of key DMS oxidation products, with moderate Nox levels (~ 0.1 ppb) leading to greater divergence than low Nox levels (~ 10 of ppt). A similar situation was found for isoprene by Archibald et al. (2010) and significant efforts have been employed to improve our understanding of isoprene oxidation through theoretical and laboratory experiments (e.g., Jenkin et al., 2015; Wennberg et al., 2018). We now focus on the role of temperature on the divergences seen thus far.

41

3.2.2 Temperature dependence of different DMS-HPMTF schemes

Figure 6 shows that even though the temperature dependence of average DMS concentration is similar across all schemes, the temperature dependence of average SO₂ and MSA concentration differs from scheme to scheme significantly. Most of the general trends were found to be similar and in line with the trends observed for the UKCA schemes and have been explained there (Section 3.1.2, **Figure 3**).

47

While WJ has the highest absolute change in HPMTF concentration throughout the temperature range (+131 ppt, +380%; **Figure 6b**), CS-H, KH, and NV show higher relative change (+43-48 pp, +763-892%). Since FG is missing the DMS oxidation by NO₃ as a potential pathway to HPMTF (via MTMP), HPMTF in FG is least affected by temperature (+34 ppt, +256%).

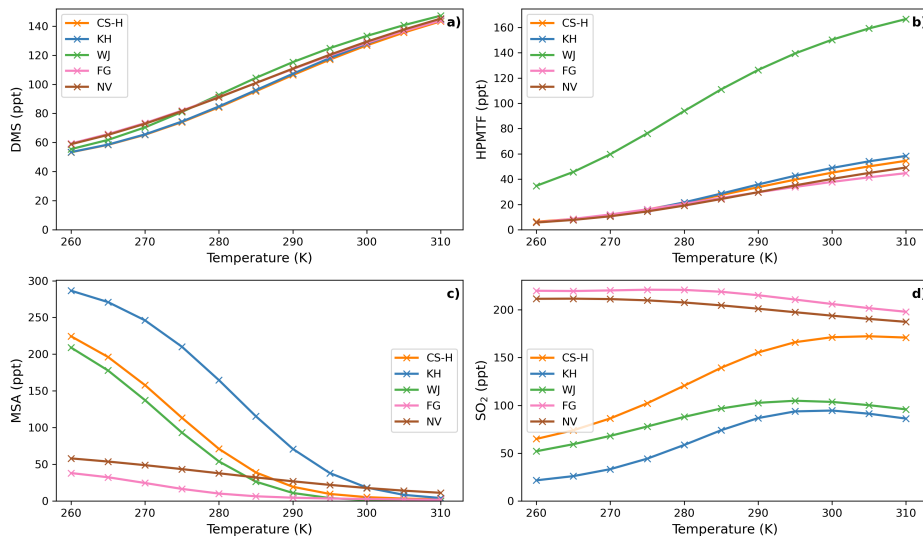
51

MSA is even more affected by temperature than HPMTF (**Figure 6c**). Its concentration shows a strong negative temperature dependence in all simulations (**Figure 6c**). The magnitude of MSA-temperature dependence differs from scheme to scheme. The smallest changes can be observed in NV (-47 ppt from 260 – 310 K), where only 25% of DMS that is oxidised through the OH-addition pathway forms MSA. Similarly in FG (-67 ppt from 260 – 310 K), where only 40% of the OH-addition

55

56 pathway forms DMSO and then potentially MSA. The largest temperature dependence can be found in the KH simulation,
57 with a change of MSA concentration of -282 ppt from 260 K to 310 K, which is very similar to CS2 (Figure 3c).
58

59 In almost all schemes, SO₂ concentration increases with temperature (Figure 6d). The greatest positive change happens
60 between the atmospheric relevant temperatures 270 and 290 K. KH and CS-H show the greatest increase in this temperature
61 range with +53 ppt (+160%) and +69 ppt (+80%), respectively (WJ: +34 ppt (51%)). Starting at 295 K, SO₂ concentration
62 plateaus with further increasing temperature and even declines slightly in some simulations (Figure 6d). NV and FG are the
63 only models which show a decrease in SO₂ throughout the entire temperature range of 260 – 310 K (NV: -24 ppt, -11%, FG:
64 -22 ppt, -10%), similar to ST~CS2 in Figure 2d. This could be due to previously mentioned simplifications in the DMS
65 additional channel, where DMSO is either completely omitted or rapidly oxidised further.
66



67
68 **Figure 6:** Temperature dependence of average (a) DMS, (b) HPMTF, (c) MSA, and (d) SO₂ concentration in different DMS
69 oxidation schemes after a quasi steady-state is reached in the box model simulation. Average Nox is approximately 10 ppt.
70

71 These results demonstrate limited consensus on gas-phase DMS oxidation, similar to the earlier work of Karl et al., 2007.
72 Importantly in the context of the role of DMS in chemistry-aerosol-climate feedbacks, we have further shown that this

73 uncertainty across mechanisms is amplified when assessing temperature sensitivity of the products of DMS oxidation. Small
74 uncertainties in the rate of reactions or the omission of intermediates can have significant effects on the resulting product
75 concentrations, as we have shown through our systematic work updating the CRI-Strat DMS scheme. All models studied tend
76 to agree on the rates of oxidation of DMS, largely controlled for by the fairly uniform treatment of the initial oxidation step.
77 However, we saw (in Figure 5) that there is large divergence at high No_x levels for MTMP and subsequently HPMTF and
78 SO_2 . In part this divergence could be reduced by better constraining the MTMP self- and cross-reactions, but in the case of
79 Fung et al. (2022) including MTMP as a product of the $\text{NO}_3 + \text{DMS}$ reaction would help it converge with the other models.
80 The effects of climate change are that it is likely that global mean surface temperature will remain higher than the pre-industrial
81 baseline for some time to come. As a result, the simulations would all suggest an increase in the amount of HPMTF formed
82 relative to other major oxidation products, especially, MSA, and most likely an overall increase in SO_2 . However, our box-
83 modelling study highlights how uncertain the situation is within the context of the current literature. At present there is a need
84 for more laboratory data and more focused sensitivity studies to isolate the major sources of uncertainty that are common
85 across DMS oxidation mechanisms and constrain them. Strikingly we see that the ST and CS2 mechanistic variants used for
86 UKCA studies span the wide range of SO_2 -Temperature and MSA-Temperature sensitivities as the recently reported updated
87 DMS mechanisms. We now move on to discuss our work implementing the CS2-H mechanism into our global chemistry-
88 climate model.

89 **4 Results from 3D model simulations using UKCA**

90 Here we present our results from the incorporation of the new CS2-H DMS mechanism described above in the 3D UKCA
91 chemistry climate model. As described in Section 2.1, we performed a series of 12-month nudged simulations with UKCA for
92 the year 2018 using 6 model simulations, with different mechanistic variants (**Table 1**). As a reminder, we use the CS2
93 simulation (Archer-Nicholls et al., 2021) as the “base” simulation, to which mechanistic improvements are made. More details
94 can be found in the SI in Section 2.

95 **4.1 Distribution of key sulfur species (DMS, HPMTF, SO_2 and sulfate).**

96 The annual mean global DMS burden was found to be between 63-66 Gg S in all model simulations. DMS concentration
97 follows a seasonal modulation with maximums in the warmer months, which coincide with phytoplankton blooms ([See the SI](#)
98 [Fig. S6a](#)). [Figure S6b](#), and [S6c](#), show the annual mean vertical profiles in the central North Atlantic region and the Southern
99 Ocean (see figure caption for bounding areas). These regions are focused on owing to the differences shown in the mixing
100 ratios of key species and the importance of these two regions to global climate (e.g., Sutton et al., 2018; Caldeira and Duffy
101 2000). In the Southern Ocean, DMS mixing ratios vary between 100 and >300 ppt. On the other hand, in the North Atlantic
102 region analysed, DMS concentrations rarely reach over 50 ppt. Here, <1 ppt DMS is found above the boundary layer (above
103 1000 m), while in the Southern Ocean DMS decreases more slowly up-to the tropopause (~8000 m). These differences in DMS

Deleted: 7a

Deleted: 7b

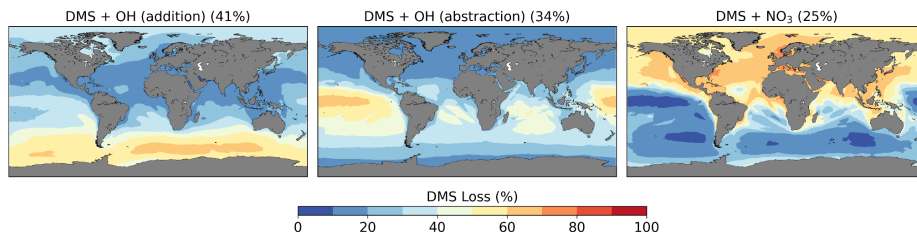
Deleted: 7c

07 distribution are a complex function of the local heterogeneity of the DMS source from the ocean and differences in the lifetime
08 of DMS due to different simulated cloud and oxidising environments (with the North Atlantic generally being a region of
09 greater oxidising capacity than the Southern Ocean (Archer-Nicholls et al., 2021; Griffiths et al., 2021)),

11 There is a significant bias in the simulated DMS mixing ratios compared with observations, which we note has been seen in
12 several other modelling studies (e.g., Fung et al. (2022)) and is driven not by the DMS chemistry but by the oceanic emissions,
13 in our case by the bias in the UKESM derived DMS emissions field (Bhatti et al., 2023). See the SI for further details.

16 4.1.1 Oxidation of DMS

17 We calculate a global average tropospheric lifetime of 1.5 days for DMS. **Figure 7** shows the global distribution of the different
18 DMS oxidation pathways in the base run (these results are not affected by the different DMS mechanism variants we use as
19 these reactions were not updated and there is only a weak feedback of DMS oxidation products on DMS oxidation itself). 75%
20 of DMS is oxidised by OH (41% via the OH-addition channel and 34% via the H-abstraction channel) and 25% by NO₃.
21 Oxidation by NO₃ is dominant in the Northern Hemisphere, especially close to the coast and over ship routes. In the Southern
22 Hemisphere, where DMS emissions are highest, the contribution is less than 20%. The addition pathway of OH oxidation is
23 favoured at lower temperatures, explaining the trend of higher DMSO formation at high latitudes.



25
26 **Figure 7:** Spatial distribution of mean percentage of DMS oxidation via DMS + OH (addition), DMS + OH (abstraction), and
27 DMS + NO₃ in the CS2 base run. The percentage in brackets denotes the contribution of this channel to the global chemical
28 loss of DMS. Only values above the ocean are shown.

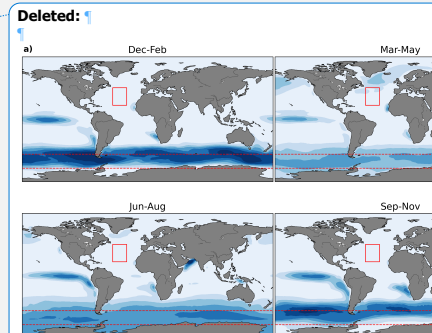


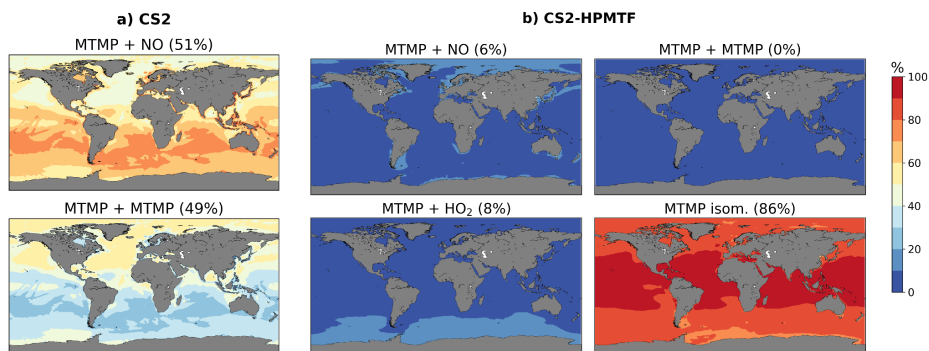
Figure 7: a) Global distribution of DMS mixing ratios in the lower troposphere (< 2 km) over the oceans in CS2. Annual mean vertical distribution of DMS in b) the Central North Atlantic (30-50°E, 20-45°N, denoted with the red rectangle in panel a) and in c) the Southern Ocean (50-70°S, denoted with the red dashed rectangle in panel a). The envelopes represent the interquartile range of the model simulation results. Note the order of magnitude difference in the DMS concentrations between the North Atlantic and Southern Ocean.

Deleted: 8

Deleted: 8

4.2 DMS Oxidation products

59% of DMS forms MTMP, the first intermediate of the abstraction pathway. In CS₂, MTMP is oxidised by NO (51%) or reacts with itself (49%) to form CH₃S (Figure 8a) which is further oxidised to SO₂, H₂SO₄, and MSA. This is clearly wrong and a failure of the CS₂ scheme. With the updates implemented in CS₂-HPMTF, 86% of MTMP isomerizes to HPMTF, while 8% is oxidised by HO₂, and only 6% by NO (Figure 8b). The self-reaction becomes negligible with the additional loss processes of MTMP, significantly lowering MTMP concentrations. The global tropospheric lifetime of MTMP is reduced from 26 min to less than one minute.



53
54 **Figure 8:** Spatial distribution of annual mean percentage of MTMP depletion (< 2 km) via MTMP + NO, its self-reaction,
55 MTMP + HO₂, and isomerization to HPMTF in a) CS₂ and b) CS₂-HPMTF. The percentage in brackets denotes the
56 contribution of this channel to the global chemical loss of MTMP. Only values above the ocean are shown.

4.2.1 Modelled HPMTF

60 In CS₂-HPMTF 51% of DMS forms HPMTF. The general patterns of the global distribution of HPMTF are similar to those
61 of DMS in Figure 9, except that relatively higher concentrations of DMS are reached in the Southern Ocean. There,
62 temperatures are lower and therefore the OH-abstraction pathway, as well as the strongly temperature-dependent isomerization
63 reaction from MTMP to HPMTF are disfavoured. At the surface, the annual mean HPMTF concentration is similar in the
64 North Atlantic and the Southern Ocean with approximately 20 ppt. However, in the North Atlantic, the variability throughout
65 space and time is greater (bigger interquartile range). Further, the vertical profiles differ visibly: In the North Atlantic HPMTF
66 concentration decreases in the boundary layer and above 2500 m HPMTF concentration is virtually zero (Figure 9h). In the

Deleted: 9a

Deleted: 9b

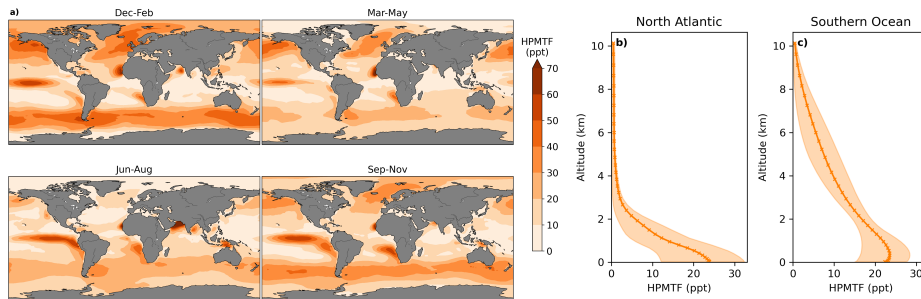
Deleted: 9

Deleted: 10

Deleted: 10b

'72 Southern Ocean, the concentration decreases more slowly and only reaches zero at 10000 m (Figure 9c). The HPMTF burden
'73 in CS2-HPMTF is 24 Gg S and HPMTF has a lifetime of 26 hours

Deleted: 10c



'75
'76 **Figure 9:** Seasonal average a) Global distribution of HPMTF mixing ratios in the lower troposphere (< 2 km) over the ocean
'77 in CS2-HPMTF. Annual means of the vertical distribution of HPMTF are shown in b) the Central North Atlantic (30-50°E,
'78 20-45°N) and c) the Southern Ocean (50-70°S). The envelopes represent the interquartile range of the model data.

Deleted: 10

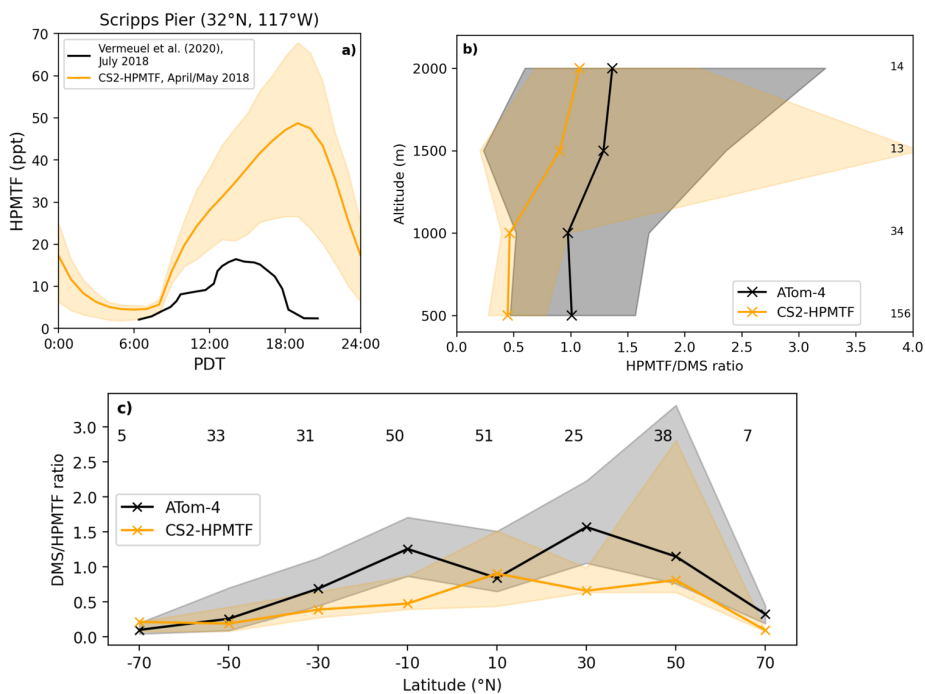
'79 **Comparison of HPMTF with observations**

'80 Since DMS in the model is likely overestimated, the same would be expected for HPMTF. Figure 10a shows that the
'81 implemented loss processes in CS2-HPMTF already lead to a diel profile of HPMTF that is similar to the one measured by
'82 Vermeuel et al. (2020) (where no DMS measurements were made), without the need to add aqueous loss or photolysis. While
'83 DMS at low altitudes was overestimated by a factor of 5 in the model (see SI), the maximum HPMTF is only 3.7 times higher
'84 than the highest measurement in the diel profile at Scripps Pier (Figure 10a). For the comparison with ATom-4 data (Figure
'85 10b,c), the DMS/HPMTF is used to account for the discrepancy between DMS concentrations observed and in the model. The
'86 model generally underestimates the HPMTF/DMS ratio. For instance, up until 1000 m, the ratio in the model is half of the
'87 measured ratio. These results indicate that loss processes of HPMTF might still be too fast in the model or the oxidation of
'88 DMS too slow. The CS2 oxidants have been evaluated before (Archer-Nicholls et al., 2021) and were found to be higher in
'89 the boundary layer than in ST simulations used in CMIP6 studies but well within the spread of other models (Griffiths et al.,
'90 2021; Stevenson et al., 2020).

Deleted: 11a

Deleted: 11a

Deleted: 11b



'98
 '99 **Figure 10:** **a)** Comparison of the diel profile of HPMTF at the Scripps Pier at the California Coast (32°N, 117°W). The
 '00 observational data (Vermeuel et al., 2020) is the mean of measurements from July 26 to August 3, 2018, while the model
 '01 output is the mean from April/May 2018. **(b)** Vertically binned (500 m) and **(c)** latitudinally binned (20°) median
 '02 DMS/HPMTF ratio along the ATom-4 flight path. The envelopes represent the interquartile range of the measurements and
 '03 the respective model results while the numbers on the side/on top give the number of measurements in the respective bin.

'04

'05 4.2.2 Modelled SO₂ and sulfate

'06 In CS2-HPMTF the SO₂ burden is increased by 5.6% compared with CS2, to 391 Gg S (Table 4). While this percentage seems
 '07 low, a significant contribution to the SO₂ burden stems from anthropogenic sources and is mainly located above the land. The
 '08 increase of SO₂ over the remote ocean, especially over the Southern Ocean, can reach up to 400% (Figure S12). At high

Deleted: 11

Deleted: 12

latitudes, the new chemistry implemented in CS2-HPMTF also introduces a stronger seasonality to SO₂, whereby SO₂ concentration is higher in respective warmer months than in CS2 (Figure S11a, Figure S12). Comparison of CS2-HPMTF with ST reveals that the SO₂ burden is 9.2% higher in the ST run, which uses a 100% SO₂ yield from DMS (Figure S9 in the SI). The global annual tropospheric sulfate burden is increased in CS2-HPMTF by 3.7% compared with CS2, to 604 Gg S. However, the sulfate burden is 5.3% higher in ST than in CS2-HPMTF (Table 4).

Comparison to observed SO₂ and sulfate

Figure 11a shows the monthly means of observed non-sea-salt sulfate (nss-sulfate) concentration at Dumont d'Urville station (66°S, 140°E) between 1991 and 1995 (Minikin et al., 1998) and compares it to the sulfate concentration in the three different UKCA model runs. The seasonal changes in sulfate concentrations are reproduced by CS2-HPMTF and ST, but not by CS2. From April to September all three runs match the observations adequately well. Earlier in the year, the results from the ST run match the observations best, while later in the year CS2-HPMTF reproduces the measurements better.

Figure 11b,c show SO₂ measurements along the ATom-4 flight path in comparison with the modelled SO₂ concentrations. In the boundary layer, all runs over-predict SO₂ in comparison to the ATom-4 data (Figure 11b). In addition to wet and dry deposition (Faloona 2009; Ranjithkumar et al., 2021), vertical mixing has been identified as a major source of uncertainty in models (Gerbig et al., 2008) and could provide an explanation for the mismatch between the simulation results and observations. At altitudes above 1.8 km, CS2-HPMTF is able to reflect SO₂ concentrations better than the other schemes. Above 9 km, the simulations underestimate SO₂, potentially indicating issues with convective transport. Overall, in the ATom-4 observations, SO₂ stays broadly constant with altitude, suggesting significant secondary sources or efficient vertical transport, while in the simulations it decreases. Additionally, the interquartile ranges of the concentrations in each bin are bigger, indicating a greater variance of model results than measured values. Overall, the mean SO₂ concentrations by the models in each latitude bin predict the mean observation values well (Figure 11c). However, the variation of values is again greater in the model, especially at low latitudes. The underestimation of SO₂ at 70°N could be due to an underestimation of the influence of anthropogenic SO₂ emissions or unrealistic deposition of SO₂ (Hardacre et al., 2021). Alternatively, the SO₂ production from DMS might be too slow still.

Deleted: 12

Deleted: S10a

Deleted: S8

Deleted: 9

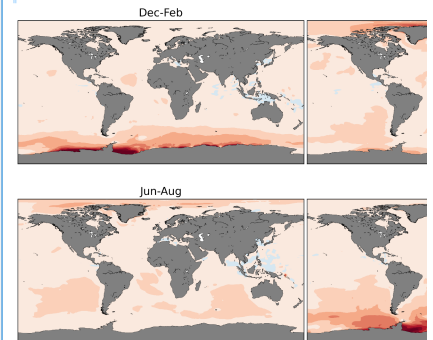


Figure 12: Relative difference in SO₂ mixing ratios in the lower troposphere (< 2 km) between CS2-HPMTF and the base run CS2 (CS2-HPMTF - CS2). Only values above the ocean are shown.

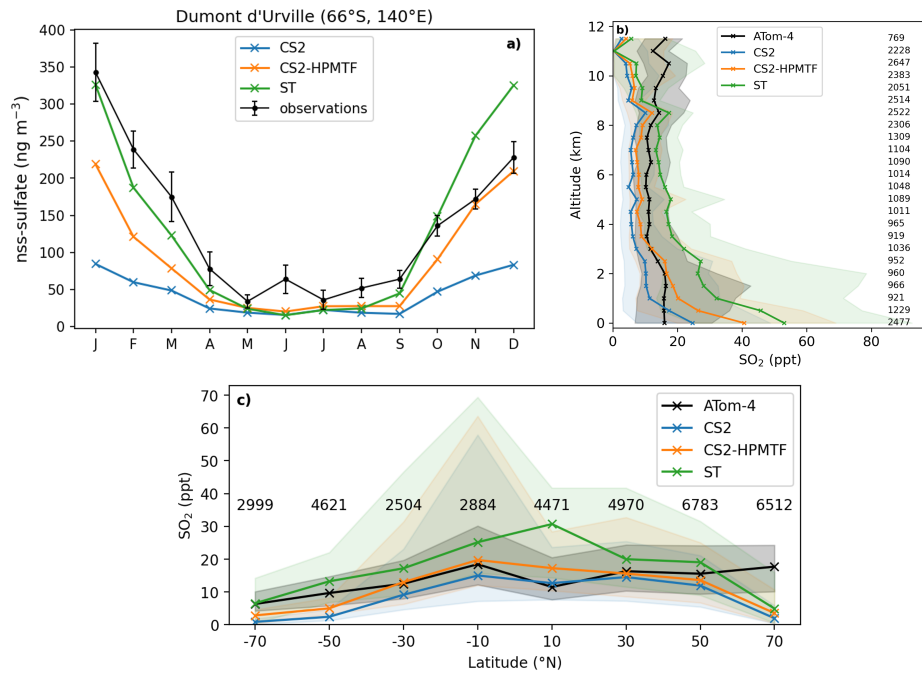
Deleted: 13a

Deleted: 13b

Deleted: 13b

Deleted: 13c

:53



:54

Figure 11: a) Comparison of nss-sulfate concentration at the Dumont d'Urville Station (66°S, 140°E) at the coast of Antarctica.

The observational data stems from Minikin et al. (1998) and represents the monthly mean concentrations and their standard deviations for the years 1991-1995. (b) Vertically binned (500 m) and (c) latitudinally binned (20°) median SO₂ mixing ratio along the ATom-4 flight path. The envelopes represent the interquartile range of the measurements and the respective model results while the numbers on the side/on top give the number of measurements in the respective bin.

:56

:57

:58

:59

:60

:61

:62

4.3 Sensitivity runs

:63

To improve our understanding of the variability of the model results, based on the uncertainties of HPMTF formation and loss, three sensitivity runs were conducted (CS2-HPMTF-CLD, CS2-HPMTF-FL, CS2-HPMTF-FP, **Table 1**). Loss of HPMTF to

:64

Deleted: 13

clouds was proposed to be a major loss pathway by Veres et al. (2020) and Vermeuel et al. (2020). CS2-HPMTF-CLD adds cloud and aqueous uptake of HPMTF with a reactive uptake coefficient, γ , of 0.01, used in the study by Novak et al. (2021). Jernigan et al. (2022) recently established a rate constant for oxidation of HPMTF by OH as $1.4 (0.27-2.4) \times 10^{-11} \text{ cm}^3 \text{ molecule}^{-1} \text{ s}^{-1}$ through constrained chamber modelling using a rate constant for the formation of HPMTF as 0.1 s^{-1} . Ye et al. (2022) also measured the rate constant for this reaction. In their study they derived a rate constant of $2.1 \times 10^{-11} \text{ cm}^3 \text{ molecule}^{-1} \text{ s}^{-1}$ and an isomerization rate constant, k_{isom} , of $0.13 \pm 0.03 \text{ s}^{-1}$ at 295 K. Whilst, further laboratory studies would be helpful in constraining the rate constant for OH + HPMTF, we recommend future work go into constraining the products of this reaction. Vermeuel et al. (2020) found the theoretically calculated rate constant $1.4 \times 10^{-12} \text{ cm}^3 \text{ molecule}^{-1} \text{ s}^{-1}$ by Wu et al. (2015) too slow and proposed a rate constant of $1.11 \times 10^{-11} \text{ cm}^3 \text{ molecule}^{-1} \text{ s}^{-1}$ instead, based on structurally similar molecules and modelling of their ground-based observations, similar to what we used in CS2-HPMTF. They recommend an upper limit of $5.1 \times 10^{-11} \text{ cm}^3 \text{ molecule}^{-1} \text{ s}^{-1}$ for the HPMTF+OH rate constant. Khan et al. (2021) and Novak et al. (2021) use $5.5 \times 10^{-11} \text{ cm}^3 \text{ molecule}^{-1} \text{ s}^{-1}$ for sensitivity tests, which was also employed in CS2-HPMTF-FL. Further, the study by Ye et al. (2021) looked at the uncertainty of the HPMTF isomerization rate. They estimate the isomerization rate constant as 0.09 s^{-1} ($0.03-0.3 \text{ s}^{-1}$, $1\sigma_g$ geometric standard deviation at 293 K). Veres et al. (2020) are on the lower end of this range (0.041 s^{-1}) and Berndt et al. (2019) at the higher end (0.23 s^{-1}). The CS2-HPMTF-FP simulation scales the rate constant of Veres et al. (2020) by a factor of 5 to match Berndt's measurements at 295 K to examine the effects of higher HPMTF production. This rate constant was also used by Wollesen de Jonge et al. (2021) in their study. The annual mean of global tropospheric burdens of relevant species in these sensitivity runs are compared in **Table 4**.

Table 4: Global annual mean tropospheric burdens of atmospheric sulfur species in UKCA base and sensitivity runs (first half of the table) and comparison to literature values (second half of the table, same acronyms as in Section 3)

Run	HPMTF burden (Gg S)	SO ₂ burden (Gg S)	Sulfate burden (Gg S)
CS2	-	370.1	582.3
ST	-	469.7	635.9
CS2-HPMTF	23.7	390.7	604.0
CS2-HPMTF-CLD	2.6	367.3	591.2
CS2-HPMTF-FL	8.9	392.6	605.6
CS2-HPMTF-FP	26.5	389.6	601.5
FG [®] (similar to CS2-HPMTF)	18	365	582
NV Base 1 [®] (similar to CS2-HPMTF)	18.8	189.0	526.7
NV Test 3 [®] (similar to CS2-HPMTF-CLD)	0.7	180.2	550.7
KH NEW_CHEM1 [®] (similar to CS2-HPMTF, with photolysis of HPMTF)	15.1	-	-
KH NEW_CHEM2 [®] (similar to CS2-HPMTF-FL)	6.1	-	-

Formatted Table

87 [Ⓢ]Fung et al., 2021; [Ⓢ]Novak et al., 2021; [Ⓢ]Khan et al., 2021.

88 4.3.1 HPMTF

89 The HPMTF burden varies between 2.6 and 26.5 Gg S among the sensitivity runs (**Table 4**). Compared to CS2-HPMTF, faster
90 OH oxidation reduces the HPMTF burden by -62% to 8.9 Gg S, while the addition of cloud and aqueous uptake to the scheme
91 reduces it by -91% to only 2.6 Gg S. Yet, a factor of 5 higher production rate constant of HPMTF only leads to a 12% increase
92 of HPMTF burden to 26.5 Gg S; suggesting that the steady-state distribution of HPMTF is controlled by the loss rate, not the
93 rate of production of HPMTF. With the isomerization rate constant recommended by Veres et al. (2020), 51% of DMS forms
94 HPMTF (86% of MTMP); with the faster rate in CS2-HPMTF-FP it is 57% (96% of MTMP). Since the use of the isomerization
95 rate from Veres et al. (2020) already outcompetes the bimolecular reactions of MTMP, scaling the A-factor does not have a
96 significant effect on the HPMTF yield from DMS. Overall, it can be estimated that globally 50-60% of DMS forms HPMTF
97 (however, if more DMS is oxidised through the addition channel by BrO or multiphase reactions, this ratio could be lower).
98 Consequently, HPMTF formation seems to be well constrained and the major uncertainties lie with the loss of HPMTF, which
99 warrant additional measurements.

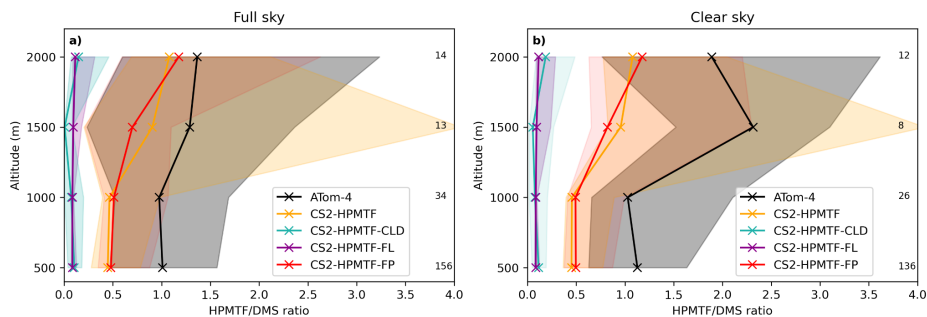
00

01 Similar to **Figure 10**, the HPMTF:DMS ratio is used in **Figure 13** to compare the results of the sensitivity model runs with
02 ATom-4 observations. In general, schemes with a higher production and slower loss of HPMTF match the observations better,
03 however, they still underestimate the measured ratios. A comparison was made to HPMTF:DMS ratios measured with no
04 clouds present. Under these clear-sky conditions, when cloud uptake of HPMTF should not play a role in the measurements,
05 observed ratios were even higher, leading to a greater difference between model results (which include clouds) and
06 observations.

07

Deleted: 11

Deleted: 14



08

Figure 13: Vertically binned (500 m) median HPMTF/DMS ratio along the ATom-4 flight path for a) full sky and b) clear sky, where measurements made in clouds are omitted. The envelopes represent the interquartile range of the measurements and the respective model results, while values on the side give the number of measurements in the respective bin. Note that the model data is the same in both panels.

4.3.2 SO₂

The SO₂ burden varies between 367.3 Gg S in CS2-HPMTF-CLD and 392.6 GgS in CS2-HPMTF-FL, suggesting that the SO₂ burden is relatively unaffected by the chemical sensitivities explored when compared with the much larger SO₂ burden simulated with ST (469.7 Gg S); mainly due to the 100% DMS-SO₂ yield (Table 4).

CS2-HPMTF, CS2-HPMTF-FL, and CS2-HPMTF-FP have a higher SO₂ burden than CS2 since the changes to the abstraction pathway (reaction 6a, 7c) and the addition of the isomerization pathway lead to more direct SO₂ production. Faster OH oxidation of HPMTF in CS2-HPMTF-FL reduces the amount of HPMTF deposited and therefore increases the SO₂ burden slightly (by 0.5%) compared to CS2-HPMTF. The faster production of HPMTF in CS2-HPMTF-FP reduces SO₂ burden marginally (-0.3%), due to more sulfur now being deposited as HPMTF or forming OCS. The addition of cloud and heterogeneous loss in CS2-HPMTF-CLD leads to immediate sulfate production instead of SO₂ formation, reducing the SO₂ burden by -6% compared to CS2-HPMTF, resulting in the lowest SO₂ burden in all runs considered.

4.4.3 Sulfate

In the sensitivity runs, the sulfate burdens are all higher than in the CS2 run (582.3 Gg S) and lower than in the ST run (635.9 Gg S). The variation by approximately 15 Gg S, from 591.2 Gg S in CS2-HPMTF-CLD to 605.6 Gg S in CS2-HPMTF-FL, is smaller than the variation in sulfate burden simulated by similar mechanistic sensitivity tests by Novak et al. (2021) (~24 Gg), suggesting some structural dependence on the results of the sensitivity tests (e.g., resolution, other model parameters). The sulfate burdens in CS2-HPMTF-FL and CS2-HPMTF-FP behave similarly to CS2-HPMTF. Since CS2-HPMTF-CLD added direct sulfate formation, a higher sulfate burden was expected. However, this was not seen in the experiments. Inspection of the sulfate aerosol distribution shows that CS2-HPMTF-CLD leads to an increase in the coarse mode sulfate and a concomitant reduction in sulfate aerosol lifetime (through an increase in wet deposition).

441 5 Discussion

442 The results described above demonstrate the global scale changes in the distribution of DMS and its oxidation products, through
443 the incorporation of improved mechanistic updates into the UKCA model. Here we discuss our results in the context of the
444 existing literature.

445 5.1 DMS

446 The DMS burden of 63-66 Gg S in this work is in good agreement with recent modelling studies (50 Gg S in Fung et al. (2022),
447 74 Gg S in Chen et al. (2018)). However, as shown in the supplement, S2.1.1, the modelled DMS concentrations do not match
448 observational measurements. One explanation could be underestimation of DMS oxidation. Here, only oxidation by OH and
449 NO₃ is included. However, Fung et al. (2022), who include oxidation by BrO, O₃ and Cl (accounting in total for 20% of DMS
450 depletion), also found that their model over-predicted DMS mixing ratios compared to the ATom-4 measurements. Inadequate
451 representation of DMS concentrations in seawater and therefore emissions contribute to the largest uncertainties in the sulfur
452 budget (Tesdal et al., 2016; Bock et al., 2021) and could explain most of the difference. Additionally, physical differences
453 between model and observation, such as wind speed and temperature, and a poor space resolution of Whole Air Sampling
454 might also play a role. Crucially, more long-term observations of DMS in the atmosphere are needed to complement works
455 that have collated oceanic DMS observations (e.g., Lana et al., 2011).

456
457 Here, in all model runs 75% of DMS is oxidised by OH and 25% by NO₃. Other studies found global contributions of OH
458 between 50-70% and NO₃ 15-30% (Boucher et al., 2003; Berglen et al., 2004; Breider et al., 2010; Khan et al., 2016; Chen et
459 al., 2018; Fung et al., 2022). The lower contribution of OH oxidation to DMS removal is explained by the addition of other
460 pathways, such as oxidation by BrO, Cl and multiphase reactions. Consequently, the lifetime of 1.5 days for DMS in this work
461 is longer than some other studies including these reactions (e.g., 0.8 days in Fung et al. (2022) and 1.2 days in Chen et al.
462 (2018)). Nonetheless, it is well within the range of 0.9 to 5 days (with a mean of 2 days) of the models examined in Faloon
463 (2009).

466 5.2 HPMTF

467 In CS2-HPMTF 51% of DMS forms HPMTF. With a faster formation of HPMTF, found in laboratory experiments, this yield
468 increases to 57% in our model. The yield could possibly be lower if other oxidation reactions of DMS are included that follow
469 the OH addition pathway (multiphase reactions, oxidation by BrO), which was omitted in this work. Veres et al. (2020), Novak
470 et al. (2021) and Fung et al. (2022) estimated that at least 30-46% of DMS was forming HPMTF, based on observationally
471 constrained modelling of *in situ* or laboratory data. Even though the rate of HPMTF formation is uncertain (Ye et al., 2021),

it does not significantly affect the HPMTF yield from DMS, since it already outcompetes most other reactions of MTMP. For HPMTF formation, uncertainty seems to lie mainly at the branching ratio of the addition and the abstraction pathway of DMS. Indeed, the uncertainty in the HPMTF burden stems from the uncertainty in the loss pathways and their respective contribution to HPMTF loss. Our model results agree well with the HPMTF burdens obtained by other global modelling studies, both in absolute values but also the relative changes we find in the sensitivity study (**Table 4**) (e.g., Fung et al. (2022)): In our sensitivity study a faster oxidation of HPMTF to OH lead to a decrease of 62% of the HPMTF burden, in Khan et al. (2021) it was 60%. In this work the addition of aqueous uptake of HPMTF reduced the burden by 91%, very similar to the reduction simulated in Novak et al. (2021) (96%).

80

81 **5.3 MSA**

82 The tropospheric MSA burden is 40 Gg S in CS2-HPMTF with a lifetime of 6 days. This falls within the range of 13-40 Gg S
83 and a lifetime of 5-7 days found in previous model studies (Pham et al., 1995; Chin et al., 1996, 2000; Cosme et al., 2002;
84 Hezel et al., 2011). However, newer studies include more multiphase processes and usually tend to have shorter lifetimes and
85 lower MSA burdens. Both the scheme in Fung et al. (2022) and Chen et al. (2018), include the loss of MSA to aqueous OH
86 oxidation, resulting in lifetimes of 0.6 days and 2.2 days and a burden of 8 Gg S and 20 Gg S, respectively.

87 **5.4 SO₂ and Sulfate**

88 Comparing SO₂ and sulfate burdens with other modelling studies is more challenging, since those species can have other
89 sources apart from DMS. That said, our SO₂ obtained in the various runs based on the CS2 scheme are comparable to Fung et
90 al. (2022), while the ST burden is significantly higher. However, the SO₂ burden from Novak et al. (2021) is much lower. This
91 difference cannot be explained solely by differences in the DMS oxidation mechanism; more likely, the difference is in
92 anthropogenic SO₂ emissions.

93 The sulfate burden in all our runs fall within the range found in other recent modelling studies (Chen et al. 2018; Novak et al.,
94 2021; Fung et al., 2022). Considering the relative change due to the addition of the isomerization pathway, the increase in
95 sulfate burden from CS2 to CS2-HPMTF is only 3.7% in our study, Fung et al. (2022) found an increase of 8.8%, when they
96 added HPMTF chemistry. However, unlike their results, we find strong seasonality in the additional sulfate produced,
97 especially in the Southern Hemisphere. The addition of cloud uptake and direct sulfate formation in CS2-HPMTF-CLD
98 decreased the sulfate burden in our study by (-)2.2%, in Novak et al. (2021) this change in mechanism lead to an increase of
99 sulfate by 4.5%.

100

101 **5.5 Comparison with BOXMOX results.**

102 In Section 3 and Section 4 we have shown the results of BOXMOX and UKCA simulations using different DMS mechanistic
103 variants respectively. Whilst the same mechanistic variants have been assessed in both model setups, it is not possible to

04 directly compare the results of the two sets of experiments because of the large differences in the model setups used. However,
05 some qualitative comparisons can be made. For MSA, Section 3.1 (**Figure 2**) suggests that the MSA simulated with CS2-
06 HPMTF should be much lower than CS2; as is calculated in Section 4.2.2 (a 70% reduction). For SO₂, both the BOXMOX
07 and UKCA results agree in the ordering of simulations, ST, CS2 and CS2-HPMTF; with ST simulating significantly more SO₂
08 than the other mechanisms. However, whereas BOXMOX simulations suggest that H₂SO₄ is predicted to be higher in CS2 and
09 CS2-HPMTF than ST, the UKCA model runs suggest that ST has the greatest burden of sulfate; highlighting the complexity
10 of making inference on aerosols from gas phase precursors in box model studies.
11

Formatted: Font: Bold

12 6 Conclusion

13 DMS remains an important molecule in our understanding of the background aerosol budget and the uncertainty of aerosols
14 to climate change (Carslaw et al., 2013). In this study we have used a combination of box modelling experiments and global
15 3D model experiments to explore the sensitivities of the DMS oxidation mechanism in the UKCA model. This work has
16 delivered a new DMS oxidation mechanism for use within the CRI-Strat framework of UKCA (Archer-Nicholls et al., 2021;
17 Weber et al., 2021), which is a significant advancement and improvement over the mechanism used in CMIP6 studies
18 (Archibald et al., 2020). Our new DMS mechanism includes many of the recently discovered and proposed oxidation pathways
19 for DMS and through the series of experiments we have performed, we have been able to benchmark this scheme against other
20 recently reported schemes in the literature. [Our results suggest that as a priority laboratory studies are performed that address](#)
21 [1\) the uptake of HPMTF onto aerosol surfaces and the products of this reaction. 2\) The kinetics and products of the following](#)
22 [reactions: CH₃SO₂ decomposition; CH₃S + O₂; CH₃SOO decomposition; CH₃SO + O₃.](#)
23

24 [However, whilst](#) future [work](#), building on the ever expanding database of laboratory studies (e.g., Ye et al., 2021; Jernigan et
25 al., 2022) are required to refine the DMS oxidation mechanism further, with the current availability of observational data, it is
26 not possible to fully constrain the [these](#) DMS oxidation [mechanisms using ambient observations](#). Hence there is a priority for
27 more observational based studies that combine ship, ground-based and aircraft platforms optimally. Fung et al. (2021) have
28 shown that there are consequences for radiative forcing by updating the DMS mechanism in the CESM model, and follow up
29 work will investigate these changes with UKCA.
30

Deleted: Whilst

Deleted: studies

Deleted: uncertain parameters in the

Deleted: mechanism

31 This study adds to the few other mechanism intercomparisons that exist in the literature, spanning back more than 25 years
32 (Capaldo and Pandis 1997; Karl et al., 2007). Similar to these other studies we find that MSA is particularly uncertain when it
33 comes to the results obtained using the range of mechanisms that we investigated. Further work should explicitly focus on
34 reducing uncertainty in the MSA budget in the atmosphere, especially given its potential importance in reconstructing paleo-
35 sea ice (Thomas et al., 2019).

140
141 In many ways, the recent advances in DMS oxidation chemistry are similar to isoprene chemistry, where over a decade ago
142 the discovery of uni-molecular isomerisation reactions resulted in a step-change in our understanding of isoprene. As with
143 isoprene, ever more complex and faithful descriptions of DMS chemistry will be delivered over the coming years. But the
144 biggest challenge (as for isoprene) will remain in reducing and accurately distilling down this complex chemistry for use in
145 global model studies, and in characterising the sources of DMS into the atmosphere (which for isoprene have only recently
146 been possibly directly e.g., Wells et al., 2020).
147

148 **Acknowledgements**

149 BAC thanks the Studienstiftung des Deutschen Volkes for financial support. We would like to thank NERC through the ACSIS
150 (NE/N018001/1) and CARES projects for funding (NE/W009412/1). We would like to thank the UK Met Office JWCRP and
151 Clean Air programmes and the National Centre for Atmospheric Science for funding the development of the UKCA model.
152 LER acknowledges support from the Deep South National Science Challenge (contract C01X1901). ATA thanks the
153 University of Canterbury Erskine Programme. This work used Monsoon2, a collaborative high-performance computing facility
154 funded by the Met Office and the Natural Environment Research Council. This work used JASMIN, the UK collaborative data
155 analysis facility.
156

157 **Competing interests**

158 The authors declare no competing interests.

159 **References**

- 160 Assaf, E., Finewax, Z., Marshall, P., Veres, P.R., Neuman, J.A. and Burkholder, J.B.: Measurement of the Intramolecular
161 Hydrogen-Shift Rate Coefficient for the CH₃SCH₂OO Radical between 314 and 433 K. *The Journal of Physical Chemistry*
162 *A*, 127(10), pp.2336-2350, 2023.
- 163 Andreae, M. O.: Ocean-atmosphere interactions in the global biogeochemical sulfur cycle, *Marine Chemistry*, 30, 1–29,
164 [https://doi.org/10.1016/0304-4203\(90\)90059-L](https://doi.org/10.1016/0304-4203(90)90059-L), 1990.
- 165 Archer-Nicholls, S., Abraham, N. L., Shin, Y. M., Weber, J., Russo, M. R., Lowe, D., Utembe, S. R., O'Connor, F. M.,
166 Kerridge, B., Latter, B., Siddans, R., Jenkin, M., Wild, O., and Archibald, A. T.: The Common Representative Intermediates
167 Mechanism Version 2 in the United Kingdom Chemistry and Aerosols Model, 13, e2020MS002420,
168 <https://doi.org/10.1029/2020MS002420>, 2021.
- 169 Archibald, A. T., Jenkin, M. E., and Shallcross, D. E.: An isoprene mechanism intercomparison, *Atmospheric Environment*,
170 44, 5356–5364, <https://doi.org/10.1016/j.atmosenv.2009.09.016>, 2010.
- 171 Archibald, A. T., O'Connor, F. M., Abraham, N. L., Archer-Nicholls, S., Chipperfield, M. P., Dalvi, M., Folberth, G. A.,
172 Dennison, F., Dhomse, S. S., Griffiths, P. T., Hardacre, C., Hewitt, A. J., Hill, R. S., Johnson, C. E., Keeble, J., Köhler, M. O.,
173 Morgenstern, O., Mulcahy, J. P., Ordóñez, C., Pope, R. J., Rumbold, S. T., Russo, M. R., Savage, N. H., Sellar, A., Stringer,
174 M., Turnock, S. T., Wild, O., and Zeng, G.: Description and evaluation of the UKCA stratosphere–troposphere chemistry
175 scheme (StratTrop vn 1.0) implemented in UKESM1, 13, 1223–1266, <https://doi.org/10.5194/gmd-13-1223-2020>, 2020.
- 176 Arsene, C., Barnes, I., and Becker, K. H.: FT-IR product study of the photo-oxidation of dimethyl sulfide: Temperature and
177 O₂ partial pressure dependence, *Phys. Chem. Chem. Phys.*, 1, 5463–5470, <https://doi.org/10.1039/A907211J>, 1999.
- 178 Atkinson, R., Baulch, D. L., Cox, R. A., Crowley, J. N., Hampson, R. F., Hynes, R. G., Jenkin, M. E., Rossi, M. J., and Troe,
179 J.: Evaluated kinetic and photochemical data for atmospheric chemistry: Volume I - gas phase reactions of O_x, HO_x, NO_x and
180 SO_x species, 4, 1461–1738, <https://doi.org/10.5194/acp-4-1461-2004>, 2004.
- 181 Barnes, I., Hjorth, J., and Mihalopoulos, N.: Dimethyl Sulfide and Dimethyl Sulfoxide and Their Oxidation in the Atmosphere,
182 *Chem. Rev.*, 106, 940–975, <https://doi.org/10.1021/cr020529+>, 2006.
- 183 Barone, S., A. Turnipseed, A., and R. Ravishankara, A.: Role of adducts in the atmospheric oxidation of dimethyl sulfide, 100,
184 39–54, <https://doi.org/10.1039/FD9950000039>, 1995.
- 185 Berglen, T. F., Berntsen, T. K., Isaksen, I. S. A., and Sundet, J. K.: A global model of the coupled sulfur/oxidant chemistry in
186 the troposphere: The sulfur cycle, 109, <https://doi.org/10.1029/2003JD003948>, 2004.

87 Berndt, T., Scholz, W., Mentler, B., Fischer, L., Hoffmann, E. H., Tilgner, A., Hyttinen, N., Prisle, N. L., Hansel, A., and
88 Herrmann, H.: Fast Peroxy Radical Isomerization and OH Recycling in the Reaction of OH Radicals with Dimethyl Sulfide,
89 J. Phys. Chem. Lett., 10, 6478–6483, <https://doi.org/10.1021/acs.jpcllett.9b02567>, 2019.

90 Bhatti, Y., Revell, L., Schuddeboom, A., McDonald, A., Archibald, A., Williams, J., Venugopal, A., Hardacre, C., and
91 Behrens, E.: The sensitivity of Southern Ocean atmospheric dimethyl sulfide to modelled sources and emissions, EGU
92 [preprint], <https://doi.org/10.5194/egusphere-2023-868>, 2023.

93 Bock, J., Michou, M., Nabat, P., Abe, M., Mulcahy, J. P., Olivié, D. J. L., Schwinger, J., Suntharalingam, P., Tjiputra, J., van
94 Hulten, M., Watanabe, M., Yool, A., and Séférian, R.: Evaluation of ocean dimethylsulfide concentration and emission in
95 CMIP6 models, 18, 3823–3860, <https://doi.org/10.5194/bg-18-3823-2021>, 2021.

96 Borissenko, D., Kukui, A., Laverdet, G., and Le Bras, G.: Experimental Study of SO₂ Formation in the Reactions of CH₃SO
97 Radical with NO₂ and O₃ in Relation with the Atmospheric Oxidation Mechanism of Dimethyl Sulfide, J. Phys. Chem. A,
98 107, 1155–1161, <https://doi.org/10.1021/jp021701g>, 2003.

99 Boucher, O., Moulin, C., Belviso, S., Aumont, O., Bopp, L., Cosme, E., von Kuhlmann, R., Lawrence, M. G., Pham, M.,
00 Reddy, M. S., Sciare, J., and Venkataraman, C.: DMS atmospheric concentrations and sulphate aerosol indirect radiative
01 forcing: a sensitivity study to the DMS source representation and oxidation, 3, 49–65, <https://doi.org/10.5194/acp-3-49-2003>,
02 2003.

03 Breider, T. J., Chipperfield, M. P., Richards, N. a. D., Carslaw, K. S., Mann, G. W., and Spracklen, D. V.: Impact of BrO on
04 dimethylsulfide in the remote marine boundary layer, 37, <https://doi.org/10.1029/2009GL040868>, 2010.

05 de Bruyn, W. J., Harvey, M., Cainey, J. M., and Saltzman, E. S.: DMS and SO₂ at Baring Head, New Zealand: Implications
06 for the Yield of SO₂ from DMS, Journal of Atmospheric Chemistry, 41, 189–209, <https://doi.org/10.1023/A:1014252106572>,
07 2002.

08 Butkovskaya, N. I. and Barnes, I.: Model Study of the Photooxidation of CH₃SO₂SCH₃ at Atmospheric Pressure: Thermal
09 Decomposition of the CH₃SO₂ Radical, in: Global Atmospheric Change and its Impact on Regional Air Quality, edited by:
10 Barnes, I., Springer Netherlands, Dordrecht, 147–152, https://doi.org/10.1007/978-94-010-0082-6_22, 2002.

11 Butkovskaya, N. I. and LeBras, G.: Mechanism of the NO₃ + DMS Reaction by Discharge Flow Mass Spectrometry, J. Phys.
12 Chem., 98, 2582–2591, <https://doi.org/10.1021/j100061a014>, 1994.

13 Caldeira, K. and Duffy, P.B. The role of the Southern Ocean in uptake and storage of anthropogenic carbon dioxide. Science,
14 287(5453), pp.620-622. 2000.

15 Campolongo, F., Saltelli, A., Jensen, N. R., Wilson, J., and Hjorth, J.: The Role of Multiphase Chemistry in the Oxidation of
16 Dimethylsulphide (DMS). A Latitude Dependent Analysis, *Journal of Atmospheric Chemistry*, 32, 327–356,
17 <https://doi.org/10.1023/A:1006154618511>, 1999.

18 Cao, J., Wang, W.L., Gao, L.J. and Fu, F.: Mechanism and thermodynamic properties of CH_3SO_3 decomposition. *Acta*
19 *Physico-Chimica Sinica*, 29(6), 1161-1167, <https://doi.org/10.3866/PKU.WHXB201304021>, 2013.

20 Capaldo, K.P. and Pandis, S.N. Dimethylsulfide chemistry in the remote marine atmosphere: Evaluation and sensitivity
21 analysis of available mechanisms. *Journal of Geophysical Research: Atmospheres*, 102(D19), pp.23251-23267. 1997

22

23 Carslaw, K. S., Lee, L. A., Reddington, C. L., Pringle, K. J., Rap, A., Forster, P. M., Mann, G. W., Spracklen, D. V.,
24 Woodhouse, M. T., Regayre, L. A., and Pierce, J. R.: Large contribution of natural aerosols to uncertainty in indirect forcing,
25 503, 67–71, <https://doi.org/10.1038/nature12674>, 2013.

26 Charlson, R. J., Lovelock, J. E., Andreae, M. O., and Warren, S. G.: Oceanic phytoplankton, atmospheric sulphur, cloud albedo
27 and climate, 326, 655–661, <https://doi.org/10.1038/326655a0>, 1987.

28 Chen, H. and Finlayson-Pitts, B. J.: New Particle Formation from Methanesulfonic Acid and Amines/Ammonia as a Function
29 of Temperature, *Environ. Sci. Technol.*, 51, 243–252, <https://doi.org/10.1021/acs.est.6b04173>, 2017.

30 Chen, H., Ezell, M. J., Arquero, K. D., Varner, M. E., Dawson, M. L., Gerber, R. B., and Finlayson-Pitts, B. J.: New particle
31 formation and growth from methanesulfonic acid, trimethylamine and water, *Phys. Chem. Chem. Phys.*, 17, 13699–13709,
32 <https://doi.org/10.1039/C5CP00838G>, 2015.

33 Chen, J., Berndt, T., Møller, K. H., Lane, J. R., and Kjaergaard, H. G.: Atmospheric Fate of the CH_3SOO Radical from the
34 $\text{CH}_3\text{S} + \text{O}_2$ Equilibrium, *J. Phys. Chem. A*, 125, 8933–8941, <https://doi.org/10.1021/acs.jpca.1c06900>, 2021.

35 Chen, Q., Sherwen, T., Evans, M., and Alexander, B.: DMS oxidation and sulfur aerosol formation in the marine troposphere:
36 a focus on reactive halogen and multiphase chemistry, 18, 13617–13637, <https://doi.org/10.5194/acp-18-13617-2018>, 2018.

37 Chin, M., Jacob, D. J., Gardner, G. M., Foreman-Fowler, M. S., Spiro, P. A., and Savoie, D. L.: A global three-dimensional
38 model of tropospheric sulfate, 101, 18667–18690, <https://doi.org/10.1029/96JD01221>, 1996.

39 Chin, M., Savoie, D. L., Huebert, B. J., Bandy, A. R., Thornton, D. C., Bates, T. S., Quinn, P. K., Saltzman, E. S., and Bruyn,
40 W. J. D.: Atmospheric sulfur cycle simulated in the global model GOCART: Comparison with field observations and regional
41 budgets, 105, 24689–24712, <https://doi.org/10.1029/2000JD900385>, 2000.

42 Collins, W. J., Lamarque, J.-F., Schulz, M., Boucher, O., Eyring, V., Hegglin, M. I., Maycock, A., Myhre, G., Prather, M.,
43 Shindell, D., and Smith, S. J.: AerChemMIP: quantifying the effects of chemistry and aerosols in CMIP6, 10, 585–607,
44 <https://doi.org/10.5194/gmd-10-585-2017>, 2017.

45 Cosme, E., Genthon, C., Martinerie, P., Boucher, O., and Pham, M.: The sulfur cycle at high-southern latitudes in the LMD-
46 ZT General Circulation Model, 107, ACH 7-1-ACH 7-19, <https://doi.org/10.1029/2002JD002149>, 2002.

47 Dee, D. P., Uppala, S. M., Simmons, A. J., Berrisford, P., Poli, P., Kobayashi, S., Andrae, U., Balmaseda, M. A., Balsamo, G.,
48 Bauer, P., Bechtold, P., Beljaars, A. C. M., van de Berg, L., Bidlot, J., Bormann, N., Delsol, C., Dragani, R., Fuentes, M.,
49 Geer, A. J., Haimberger, L., Healy, S. B., Hersbach, H., Hólm, E. V., Isaksen, I., Kållberg, P., Köhler, M., Matricardi, M.,
50 McNally, A. P., Monge-Sanz, B. M., Morcrette, J.-J., Park, B.-K., Peubey, C., de Rosnay, P., Tavolato, C., Thépaut, J.-N., and
51 Vitart, F.: The ERA-Interim reanalysis: configuration and performance of the data assimilation system, 137, 553–597,
52 <https://doi.org/10.1002/qj.828>, 2011.

53 Faloon, T.: Sulfur processing in the marine atmospheric boundary layer: A review and critical assessment of modeling
54 uncertainties, *Atmospheric Environment*, 43, 2841–2854, <https://doi.org/10.1016/j.atmosenv.2009.02.043>, 2009.

55 Fung, K. M., Heald, C. L., Kroll, J. H., Wang, S., Jo, D. S., Gettelman, A., Lu, Z., Liu, X., Zaveri, R. A., Apel, E., Blake, D.
56 R., Jimenez, J.-L., Campuzano-Jost, P., Veres, P., Bates, T. S., Shilling, J. E., and Zawadowicz, M.: Exploring DMS oxidation
57 and implications for global aerosol radiative forcing, 1–58, <https://doi.org/10.5194/acp-2021-782>, 2021.

58 Gali, M., Levasseur, M., Devred, E., Simó, R., and Babin, M.: Sea-surface dimethylsulfide (DMS) concentration from satellite
59 data at global and regional scales, *Biogeosciences*, 15, 3497–3519, <https://doi.org/10.5194/bg-15-3497-2018>, 2018.

60 Glasow, R. von, Sander, R., Bott, A., and Crutzen, P. J.: Modeling halogen chemistry in the marine boundary layer 1. Cloud-
61 free MBL, 107, ACH 9-1-ACH 9-16, <https://doi.org/10.1029/2001JD000942>, 2002.

62 Griffiths, P. T., Murray, L. T., Zeng, G., Shin, Y. M., Abraham, N. L., Archibald, A. T., Deushi, M., Emmons, L. K., Galbally,
63 I. E., Hassler, B., Horowitz, L. W., Keeble, J., Liu, J., Moeini, O., Naik, V., O'Connor, F. M., Oshima, N., Tarasick, D., Tilmes,
64 S., Turnock, S. T., Wild, O., Young, P. J., and Zanis, P.: Tropospheric ozone in CMIP6 simulations, *Atmos. Chem. Phys.*, 21,
65 4187–4218, <https://doi.org/10.5194/acp-21-4187-2021>, 2021.

66 Guenther, A. B., Jiang, X., Heald, C. L., Sakulyanontvittaya, T., Duhl, T., Emmons, L. K., and Wang, X.: The Model of
67 Emissions of Gases and Aerosols from Nature version 2.1 (MEGAN2.1): an extended and updated framework for modeling
68 biogenic emissions, 5, 1471–1492, <https://doi.org/10.5194/gmd-5-1471-2012>, 2012.

69 Hezel, P. J., Alexander, B., Bitz, C. M., Steig, E. J., Holmes, C. D., Yang, X., and Sciare, J.: Modeled methanesulfonic acid
70 (MSA) deposition in Antarctica and its relationship to sea ice, 116, <https://doi.org/10.1029/2011JD016383>, 2011.

71 Ho, S., Peng, L., Anthes, R. A., Kuo, Y.-H., and Lin, H.-C.: Marine Boundary Layer Heights and Their Longitudinal, Diurnal,
72 and Interseasonal Variability in the Southeastern Pacific Using COSMIC, CALIOP, and Radiosonde Data, *J. Climate*, 28,
73 2856–2872, <https://doi.org/10.1175/JCLI-D-14-00238.1>, 2015.

74 Hoesly, R. M., Smith, S. J., Feng, L., Klimont, Z., Janssens-Maenhout, G., Pitkanen, T., Seibert, J. J., Vu, L., Andres, R. J.,
75 Bolt, R. M., Bond, T. C., Dawidowski, L., Kholod, N., Kurokawa, J., Li, M., Liu, L., Lu, Z., Moura, M. C. P., O'Rourke, P.
76 R., and Zhang, Q.: Historical (1750–2014) anthropogenic emissions of reactive gases and aerosols from the Community
77 Emissions Data System (CEDS), 11, 369–408, <https://doi.org/10.5194/gmd-11-369-2018>, 2018.

78 Hoffmann, E. H., Tilgner, A., Schrödner, R., Bräuer, P., Wolke, R., and Herrmann, H.: An advanced modeling study on the
79 impacts and atmospheric implications of multiphase dimethyl sulfide chemistry, *PNAS*, 113, 11776–11781,
80 <https://doi.org/10.1073/pnas.1606320113>, 2016.

81 Hoffmann, E. H., Heinold, B., Kubin, A., Tegen, I., and Herrmann, H.: The Importance of the Representation of DMS
82 Oxidation in Global Chemistry-Climate Simulations, 48, e2021GL094068, <https://doi.org/10.1029/2021GL094068>, 2021.

83 Hulswar, S., Simó, R., Galí, M., Bell, T. G., Lana, A., Inamdar, S., Halloran, P. R., Manville, G., and Mahajan, A. S.: Third
84 revision of the global surface seawater dimethyl sulfide climatology (DMS-Rev3), *Earth Syst. Sci. Data*, 14, 2963–2987,
85 <https://doi.org/10.5194/essd-14-2963-2022>, 2022.

86 Jenkin, M. E., Young, J. C., and Rickard, A. R.: The MCM v3.3.1 degradation scheme for isoprene, 15, 11433–11459,
87 <https://doi.org/10.5194/acp-15-11433-2015>, 2015.

88 Jenkin, M. E., Khan, M. A. H., Shallcross, D. E., Bergström, R., Simpson, D., Murphy, K. L. C., and Rickard, A. R.: The CRI
89 v2.2 reduced degradation scheme for isoprene, *Atmospheric Environment*, 212, 172–182,
90 <https://doi.org/10.1016/j.atmosenv.2019.05.055>, 2019.

91 Jernigan, C.M., Fite, C.H., Vereecken, L., Berkelhammer, M.B., Rollins, A.W., Rickly, P.S., Novelli, A., Taraborrelli, D.,
92 Holmes, C.D. and Bertram, T.H. Efficient Production of Carbonyl Sulfide in the Low-NOx Oxidation of Dimethyl Sulfide.
93 *Geophysical Research Letters*, 49(3), p.e2021GL096838. 2022.

94 Karl, M., Gross, A., Leck, C., and Pirjola, L.: Intercomparison of dimethylsulfide oxidation mechanisms for the marine
95 boundary layer: Gaseous and particulate sulfur constituents, 112, <https://doi.org/10.1029/2006JD007914>, 2007.

96 Khan, M. A. H., Gillespie, S. M. P., Razi, B., Xiao, P., Davies-Coleman, M. T., Percival, C. J., Derwent, R. G., Dyke, J. M.,
97 Ghosh, M. V., Lee, E. P. F., and Shallcross, D. E.: A modelling study of the atmospheric chemistry of DMS using the global
98 model, STOCHEM-CRI, *Atmospheric Environment*, 127, 69–79, <https://doi.org/10.1016/j.atmosenv.2015.12.028>, 2016.

99 Khan, M. A. H., Bannan, T. J., Holland, R., Shallcross, D. E., Archibald, A. T., Matthews, E., Back, A., Allan, J., Coe, H.,
00 Artaxo, P., and Percival, C. J.: Impacts of Hydroperoxymethyl Thioformate on the Global Marine Sulfur Budget, *ACS Earth*
01 *Space Chem.*, 5, 2577–2586, <https://doi.org/10.1021/acsearthspacechem.1c00218>, 2021.

02 Knote, C., Tuccella, P., Curci, G., Emmons, L., Orlando, J. J., Madronich, S., Baró, R., Jiménez-Guerrero, P., Luecken, D.,
03 Hogrefe, C., Forkel, R., Werhahn, J., Hirtl, M., Pérez, J. L., San José, R., Giordano, L., Brunner, D., Yahya, K., and Zhang,
04 Y.: Influence of the choice of gas-phase mechanism on predictions of key gaseous pollutants during the AQMEII phase-2
05 intercomparison, *Atmospheric Environment*, 115, 553–568, <https://doi.org/10.1016/j.atmosenv.2014.11.066>, 2015.

06 Lee, C., Martin, R. V., van Donkelaar, A., Lee, H., Dickerson, R. R., Hains, J. C., Krotkov, N., Richter, A., Vinnikov, K., and
07 Schwab, J. J.: SO₂ emissions and lifetimes: Estimates from inverse modeling using in situ and global, space-based
08 (SCIAMACHY and OMI) observations, *J. Geophys. Res.-Atmos.*, 116, D06304, <https://doi.org/10.1029/2010JD014758>,
09 2011.

10 McKee, M. L.: Theoretical study of the CH₃SOO radical, *Chemical Physics Letters*, 211, 643–648,
11 [https://doi.org/10.1016/0009-2614\(93\)80157-K](https://doi.org/10.1016/0009-2614(93)80157-K), 1993.

12 Minikin, A., Legrand, M., Hall, J., Wagenbach, D., Kleefeld, C., Wolff, E., Pasteur, E. C., and Ducroz, F.: Sulfur-containing
13 species (sulfate and methanesulfonate) in coastal Antarctic aerosol and precipitation, 103, 10975–10990,
14 <https://doi.org/10.1029/98JD00249>, 1998.

15 Mulcahy, J.P., Jones, C., Sellar, A., Johnson, B., Boutle, I.A., Jones, A., Andrews, T., Rumbold, S.T., Mollard, J., Bellouin,
16 N. and Johnson, C.E. Improved aerosol processes and effective radiative forcing in HadGEM3 and UKESM1. *Journal of*
17 *Advances in Modeling Earth Systems*, 10(11), pp.2786-2805. 2018.

18 Mulcahy, J. P., Johnson, C., Jones, C. G., Povey, A. C., Scott, C. E., Sellar, A., Turnock, S. T., Woodhouse, M. T., Abraham,
19 N. L., Andrews, M. B., Bellouin, N., Browse, J., Carslaw, K. S., Dalvi, M., Folberth, G. A., Glover, M., Grosvenor, D. P.,
20 Hardacre, C., Hill, R., Johnson, B., Jones, A., Kipling, Z., Mann, G., Mollard, J., O'Connor, F. M., Palmiéri, J., Reddington,
21 C., Rumbold, S. T., Richardson, M., Schutgens, N. A. J., Stier, P., Stringer, M., Tang, Y., Walton, J., Woodward, S., and Yool,
22 A.: Description and evaluation of aerosol in UKESM1 and HadGEM3-GC3.1 CMIP6 historical simulations, 13, 6383–6423,
23 <https://doi.org/10.5194/gmd-13-6383-2020>, 2020.

24 Novak, G. A., Fite, C. H., Holmes, C. D., Veres, P. R., Neuman, J. A., Faloon, I., Thornton, J. A., Wolfe, G. M., Vermeuel,
25 M. P., Jernigan, C. M., Peischl, J., Ryerson, T. B., Thompson, C. R., Bourgeois, I., Warneke, C., Gkatzelis, G. I., Coggon, M.
26 M., Sekimoto, K., Bui, T. P., Dean-Day, J., Diskin, G. S., DiGangi, J. P., Nowak, J. B., Moore, R. H., Wiggins, E. B., Winstead,
27 E. L., Robinson, C., Thornhill, K. L., Sanchez, K. J., Hall, S. R., Ullmann, K., Dollner, M., Weinzierl, B., Blake, D. R., and
28 Bertram, T. H.: Rapid cloud removal of dimethyl sulfide oxidation products limits SO₂ and cloud condensation nuclei
29 production in the marine atmosphere, *PNAS*, 118, <https://doi.org/10.1073/pnas.2110472118>, 2021.

30 Pacifico, F., Harrison, S. P., Jones, C. D., Arneth, A., Sitch, S., Weedon, G. P., Barkley, M. P., Palmer, P. I., Serça, D.,
31 Potosnak, M., Fu, T.-M., Goldstein, A., Bai, J., and Schurgers, G.: Evaluation of a photosynthesis-based biogenic isoprene
32 emission scheme in JULES and simulation of isoprene emissions under present-day climate conditions, 11, 4371–4389,
33 <https://doi.org/10.5194/acp-11-4371-2011>, 2011.

34 Pham, M., Müller, J.-F., Brasseur, G. P., Granier, C., and Mégie, G.: A three-dimensional study of the tropospheric sulfur
35 cycle, 100, 26061–26092, <https://doi.org/10.1029/95JD02095>, 1995.

36 Ranjithkumar, A., Gordon, H., Williamson, C., Rollins, A., Pringle, K., Kupc, A., Abraham, N. L., Brock, C., and Carslaw,
37 K.: Constraints on global aerosol number concentration, SO₂ and condensation sink in UKESM1 using ATom measurements,
38 Atmos. Chem. Phys., 21, 4979–5014, <https://doi.org/10.5194/acp-21-4979-2021>, 2021.

39 Sander, R.: Compilation of Henry's law constants (version 4.0) for water as solvent, Atmos. Chem. Phys., 15, 4399–4981,
40 <https://doi.org/10.5194/acp-15-4399-2015>, 2015, corrigendum, 2021.

41 Sandu, A. and Sander, R.: Technical note: Simulating chemical systems in Fortran90 and Matlab with the Kinetic PreProcessor
42 KPP-2.1, 6, 187–195, <https://doi.org/10.5194/acp-6-187-2006>, 2006.

43 Sciare, J., Mihalopoulos, N., and Dentener, F. J.: Interannual variability of atmospheric dimethylsulfide in the southern Indian
44 Ocean, J. Geophys. Res., 105, 26369–26377, <https://doi.org/10.1029/2000JD900236>, 2000.

45 Sciare, J., Baboukas, E., and Mihalopoulos, N.: Short-Term Variability of Atmospheric DMS and Its Oxidation Products at
46 Amsterdam Island during Summer Time, Journal of Atmospheric Chemistry, 39, 281–302,
47 <https://doi.org/10.1023/A:1010631305307>, 2001.

48 Sellar, A. A., Jones, C. G., Mulcahy, J. P., Tang, Y., Yool, A., Wiltshire, A., O'Connor, F. M., Stringer, M., Hill, R., Palmieri,
49 J., Woodward, S., Mora, L. de, Kuhlbrodt, T., Rumbold, S. T., Kelley, D. I., Ellis, R., Johnson, C. E., Walton, J., Abraham, N.
50 L., Andrews, M. B., Andrews, T., Archibald, A. T., Berthou, S., Burke, E., Blockley, E., Carslaw, K., Dalvi, M., Edwards, J.,
51 Folberth, G. A., Gedney, N., Griffiths, P. T., Harper, A. B., Hendry, M. A., Hewitt, A. J., Johnson, B., Jones, A., Jones, C. D.,
52 Keeble, J., Liddicoat, S., Morgenstern, O., Parker, R. J., Predoi, V., Robertson, E., Siahahaan, A., Smith, R. S., Swaminathan,
53 R., Woodhouse, M. T., Zeng, G., and Zerroukat, M.: UKESM1: Description and Evaluation of the U.K. Earth System Model,
54 11, 4513–4558, <https://doi.org/10.1029/2019MS001739>, 2019.

55 Sellar, A. A., Walton, J., Jones, C. G., Wood, R., Abraham, N. L., Andrejczuk, M., Andrews, M. B., Andrews, T., Archibald,
56 A. T., de Mora, L., Dyson, H., Elkington, M., Ellis, R., Florek, P., Good, P., Gohar, L., Haddad, S., Hardiman, S. C., Hogan,
57 E., Iwi, A., Jones, C. D., Johnson, B., Kelley, D. I., Kettleborough, J., Knight, J. R., Köhler, M. O., Kuhlbrodt, T., Liddicoat,
58 S., Linova-Pavlova, I., Mizielinski, M. S., Morgenstern, O., Mulcahy, J., Neiningner, E., O'Connor, F. M., Petrie, R., Ridley,
59 J., Rioual, J.-C., Roberts, M., Robertson, E., Rumbold, S., Seddon, J., Shepherd, H., Shim, S., Stephens, A., Teixeira, J. C.,
60 Tang, Y., Williams, J., Wiltshire, A., and Griffiths, P. T.: Implementation of U.K. Earth System Models for CMIP6, 12,
61 e2019MS001946, <https://doi.org/10.1029/2019MS001946>, 2020.

.62 Stevenson, D. S., Zhao, A., Naik, V., O'Connor, F. M., Tilmes, S., Zeng, G., Murray, L. T., Collins, W. J., Griffiths, P. T.,
.63 Shim, S., Horowitz, L. W., Sentman, L. T., and Emmons, L.: Trends in global tropospheric hydroxyl radical and methane
.64 lifetime since 1850 from AerChemMIP, *Atmos. Chem. Phys.*, 20, 12905–12920, <https://doi.org/10.5194/acp-20-12905-2020>,
.65 2020.

.66 Sutton, R.T., McCarthy, G.D., Robson, J., Sinha, B., Archibald, A.T. and Gray, L.J. Atlantic multidecadal variability and the
.67 UK ACSIS program. *Bulletin of the American Meteorological Society*, 99(2), pp.415-425. 2018.

.68 Telford, P. J., Abraham, N. L., Archibald, A. T., Braesicke, P., Dalvi, M., Morgenstern, O., O'Connor, F. M., Richards, N. a.
.69 D., and Pyle, J. A.: Implementation of the Fast-JX Photolysis scheme (v6.4) into the UKCA component of the MetUM
.70 chemistry-climate model (v7.3), 6, 161–177, <https://doi.org/10.5194/gmd-6-161-2013>, 2013.

.71 Tesdal, J.-E., Christian, J. R., Monahan, A. H., Salzen, K. von, Tesdal, J.-E., Christian, J. R., Monahan, A. H., and Salzen, K.
.72 von: Evaluation of diverse approaches for estimating sea-surface DMS concentration and air–sea exchange at global scale,
.73 *Environ. Chem.*, 13, 390–412, <https://doi.org/10.1071/EN14255>, 2015.

.74 Thomas, E.R., Allen, C.S., Etourneau, J., King, A.C., Severi, M., Winton, V.H.L., Mueller, J., Crosta, X. and Peck, V.L.
.75 Antarctic sea ice proxies from marine and ice core archives suitable for reconstructing sea ice over the past 2000 years.
.76 *Geosciences*, 9(12), 506. 2019.

.77 Turnipseed, A. A., Barone, S. B., and Ravishankara, A. R.: Observation of methylthiyl radical addition to oxygen in the gas
.78 phase, *J. Phys. Chem.*, 96, 7502–7505, <https://doi.org/10.1021/j100198a006>, 1992.

.79 Urbanski, S. P., Stickel, R. E., and Wine, P. H.: Mechanistic and Kinetic Study of the Gas-Phase Reaction of Hydroxyl Radical
.80 with Dimethyl Sulfoxide, *J. Phys. Chem. A*, 102, 10522–10529, <https://doi.org/10.1021/jp9833911>, 1998.

.81 Veres, P. R., Neuman, J. A., Bertram, T. H., Assaf, E., Wolfe, G. M., Williamson, C. J., Weinzierl, B., Tilmes, S., Thompson,
.82 C. R., Thames, A. B., Schroder, J. C., Saiz-Lopez, A., Rollins, A. W., Roberts, J. M., Price, D., Peischl, J., Nault, B. A., Møller,
.83 K. H., Miller, D. O., Meinardi, S., Li, Q., Lamarque, J.-F., Kupc, A., Kjaergaard, H. G., Kinnison, D., Jimenez, J. L., Jernigan,
.84 C. M., Hornbrook, R. S., Hills, A., Dollner, M., Day, D. A., Cuevas, C. A., Campuzano-Jost, P., Burkholder, J., Bui, T. P.,
.85 Brune, W. H., Brown, S. S., Brock, C. A., Bourgeois, I., Blake, D. R., Apel, E. C., and Ryerson, T. B.: Global airborne sampling
.86 reveals a previously unobserved dimethyl sulfide oxidation mechanism in the marine atmosphere, *Proc Natl Acad Sci USA*,
.87 117, 4505–4510, <https://doi.org/10.1073/pnas.1919344117>, 2020.

.88 Vermeuel, M. P., Novak, G. A., Jernigan, C. M., and Bertram, T. H.: Diel Profile of Hydroperoxymethyl Thioformate:
.89 Evidence for Surface Deposition and Multiphase Chemistry, *Environ. Sci. Technol.*, 54, 12521–12529,
.90 <https://doi.org/10.1021/acs.est.0c04323>, 2020.

.91 von Glasow, R. and Crutzen, P. J.: Model study of multiphase DMS oxidation with a focus on halogens, *Atmos. Chem. Phys.*,
.92 4, 589–608, <https://doi.org/10.5194/acp-4-589-2004>, 2004.

.93 Walters, D., Baran, A. J., Boutle, I., Brooks, M., Earnshaw, P., Edwards, J., Furtado, K., Hill, P., Lock, A., Manners, J.,
.94 Morcrette, C., Mulcahy, J., Sanchez, C., Smith, C., Stratton, R., Tennant, W., Tomassini, L., Van Weverberg, K., Vosper, S.,
.95 Willett, M., Browse, J., Bushell, A., Carslaw, K., Dalvi, M., Essery, R., Gedney, N., Hardiman, S., Johnson, B., Johnson, C.,
.96 Jones, A., Jones, C., Mann, G., Milton, S., Rumbold, H., Sellar, A., Ujiie, M., Whittall, M., Williams, K., and Zerroukat, M.:
.97 The Met Office Unified Model Global Atmosphere 7.0/7.1 and JULES Global Land 7.0 configurations, 12, 1909–1963,
.98 <https://doi.org/10.5194/gmd-12-1909-2019>, 2019.

.99 Wang, X., Jacob, D. J., Downs, W., Zhai, S., Zhu, L., Shah, V., Holmes, C. D., Sherwen, T., Alexander, B., Evans, M. J.,
.00 Eastham, S. D., Neuman, J. A., Veres, P. R., Koenig, T. K., Volkamer, R., Huey, L. G., Bannan, T. J., Percival, C. J., Lee, B.
.01 H., and Thornton, J. A.: Global tropospheric halogen (Cl, Br, I) chemistry and its impact on oxidants, 21, 13973–13996,
.02 <https://doi.org/10.5194/acp-21-13973-2021>, 2021.

.03 Weber, J., Archer-Nicholls, S., Griffiths, P., Berndt, T., Jenkin, M., Gordon, H., Knote, C., and Archibald, A. T.: CRI-HOM:
.04 A novel chemical mechanism for simulating highly oxygenated organic molecules (HOMs) in global chemistry–aerosol–
.05 climate models, *Atmos. Chem. Phys.*, 20, 10889–10910, <https://doi.org/10.5194/acp-20-10889-2020>, 2020.

.06 Weber, J., Archer-Nicholls, S., Abraham, N. L., Shin, Y. M., Bannan, T. J., Percival, C. J., Bacak, A., Artaxo, P., Jenkin, M.,
.07 Khan, M. A. H., Shallcross, D. E., Schwantes, R. H., Williams, J., and Archibald, A. T.: Improvements to the representation
.08 of BVOC chemistry–climate interactions in UKCA (v11.5) with the CRI-Strat 2 mechanism: incorporation and evaluation, 14,
.09 5239–5268, <https://doi.org/10.5194/gmd-14-5239-2021>, 2021.

.10 Wells, K.C., Millet, D.B., Payne, V.H., Deventer, M.J., Bates, K.H., de Gouw, J.A., Graus, M., Warneke, C., Wisthaler, A.,
.11 and Fuentes, J.D. Satellite isoprene retrievals constrain emissions and atmospheric oxidation. *Nature*, 585(7824), 225-233.
.12 2020.

.13 Wennberg, P. O., Bates, K. H., Crounse, J. D., Dodson, L. G., McVay, R. C., Mertens, L. A., Nguyen, T. B., Praske, E.,
.14 Schwantes, R. H., Smarte, M. D., St Clair, J. M., Teng, A. P., Zhang, X., and Seinfeld, J. H.: Gas-Phase reactions of isoprene
.15 and its major oxidation products, *Chem. Rev.*, 118, 3337–3390, <https://doi.org/10.1021/acs.chemrev.7b00439>, 2018.

.16 Wofsy, S. C., Afshar, S., Allen, H. M., Apel, E. C., Asher, E. C., Barletta, B., Bent, J., Bian, H., Biggs, B. C., Blake, D. R.,
.17 Blake, N., Bourgeois, I., Brock, C. A., Brune, W. H., Budney, J. W., Bui, T. P., Butler, A., Campuzano-Jost, P., Chang, C. S.,
.18 Chin, M., Commane, R., Corr, G., and Zeng, L. H.: ATom: merged atmospheric chemistry, trace gases, and aerosols, data set,
.19 ORNL DAAC, Oak Ridge, Tennessee, USA, <https://doi.org/10.3334/ORNLDAAC/1581>, 2018.

.20 Wollesen de Jonge, R., Elm, J., Rosati, B., Christiansen, S., Hyttinen, N., Lüdemann, D., Bilde, M., and Roldin, P.: Secondary
.21 aerosol formation from dimethyl sulfide – improved mechanistic understanding based on smog chamber experiments and
.22 modelling, 21, 9955–9976, <https://doi.org/10.5194/acp-21-9955-2021>, 2021.

23 Wu, R., Wang, S., and Wang, L.: New Mechanism for the Atmospheric Oxidation of Dimethyl Sulfide. The Importance of
24 Intramolecular Hydrogen Shift in a $\text{CH}_3\text{SCH}_2\text{OO}$ Radical, *J. Phys. Chem. A*, 119, 112–117, <https://doi.org/10.1021/jp511616j>,
25 2015.

26 Ye, Q., Goss, M. B., Isaacman-VanWertz, G., Zaytsev, A., Massoli, P., Lim, C., Croteau, P., Canagaratna, M., Knopf, D. A.,
27 Keutsch, F. N., Heald, C. L., and Kroll, J. H.: Organic Sulfur Products and Peroxy Radical Isomerization in the OH Oxidation
28 of Dimethyl Sulfide, *ACS Earth Space Chem.*, <https://doi.org/10.1021/acsearthspacechem.1c00108>, 2021.
29

Page 9: [1] Deleted A. T. Archibald 01/09/2023 12:33:00



Page 9: [2] Deleted A. T. Archibald 01/09/2023 12:33:00



Page 9: [3] Deleted A. T. Archibald 01/09/2023 12:33:00

